SAND2019-15457PE

Sandia National Laboratories

An Evolution of a Mindset: A Historical Perspective on Sandia National Laboratories Fire Science Philosophy

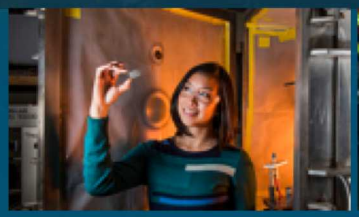

Stanford ICME Seminar Series
January 14th, 2020 Stanford University

PRESENTED BY

Stefan Domino, Ph.D.

Computational Thermal & Fluid Mechanics

Sandia National Laboratories SAND2020-TBD

Sandia National Laboratories is a multimission laboratory managed and operated by National Technology & Engineering Solutions of Sandia, LLC, a wholly owned subsidiary of Honeywell International Inc., for the U.S. Department of Energy's National Nuclear Security Administration under contract DE-NA0003525.

Presentation Objectives

- Pool Fire Heat Transfer Mechanisms
- Physics Overview
- Evolution from Quiescent, to Crossflow, to Whirling
- Turbulence Modeling Choices
- Solution Verification Concepts Demonstrated
- Coupling and Discretization Overview
- Conclusions

- Interleaved Research Thrust Concepts:
  - Automatic Structural Uncertainty Approaches
  - Fire Dynamics in Crossflow
  - Higher-order numerics
  - Extreme-scale computing
  - Machine Learning for Wall-Modeled Large-Eddy Simulation (LES)

To be Human is to Intuitively Understand the Dynamics of Fire

- Evidence of cooked food dates back ~two million years, Gowlett and Wrangham *Azania: Archaeological Research in Africa,* 2013
- The first example of controlled fire usage could date back ~one million years, Bowman et al., *Science*, 2009
- Widespread evidence of usage ~100,000 years ago
- Therefore, humans have an *innate* understanding of how fire sounds, feels, and behaves

10 meter outdoor fire (Nikos)

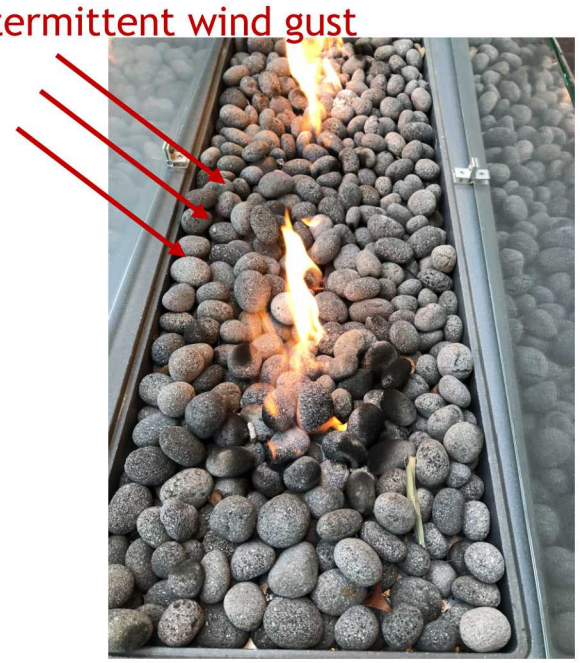

Fire feature soot plating

Heat Transfer Mechanisms: Abnormal/Thermal Environment (ATE)

- Characterized by a highly sooting, turbulent reacting flow with participating media radiation (PMR) and conjugate heat transfer (CHT) *multi-physics* coupling
- Liquid fuels, e.g., JP-8, are common due to its usage in transportation, however, propellants (point-Lagrangian/Eulerian) and composite (heterogeneous combustion) also encompass the ATE

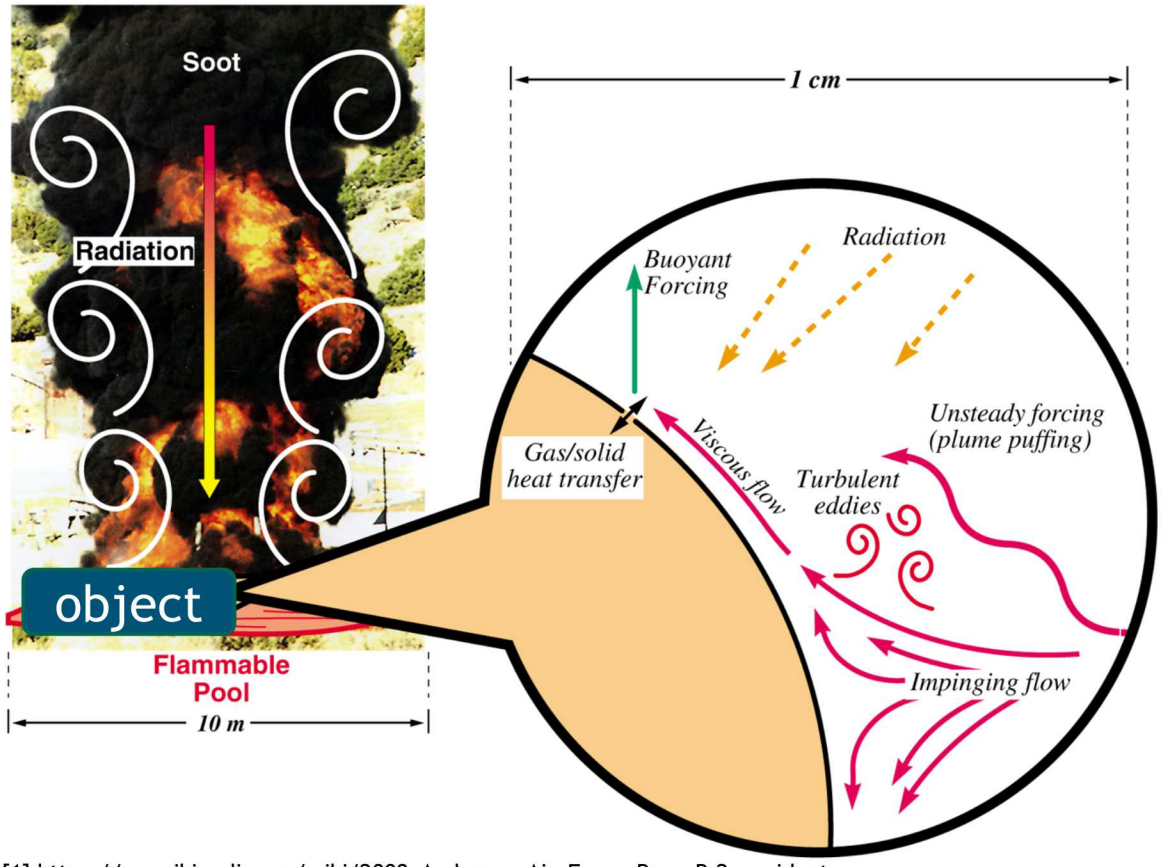

Propellant upward burn

[1]

Anderson Air Force B-2 Accident (2/2008)

[1] https://en.wikipedia.org/wiki/2008_Andersen_Air_Force_Base_B-2_accident

Grand Challenge: Vast Disparity in Time- and Length-Scales

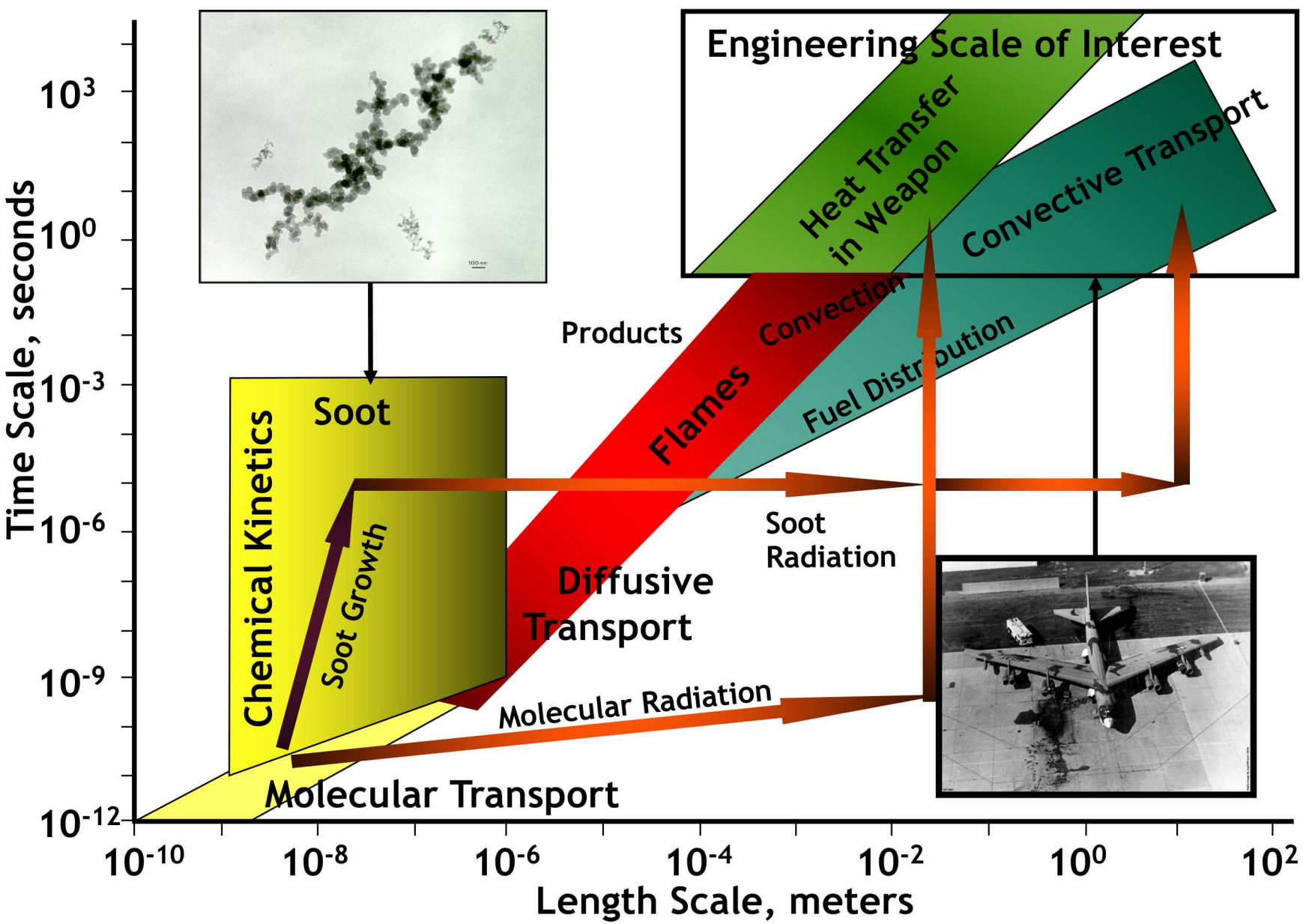

Evolution of a Mindset …. Quiescence

"There is no better, there is no more open door by which you can enter into the study of natural philosophy, than by considering the physical phenomena of a candle"

The Chemical History of a Candle, Michael Faraday (1791-1867)

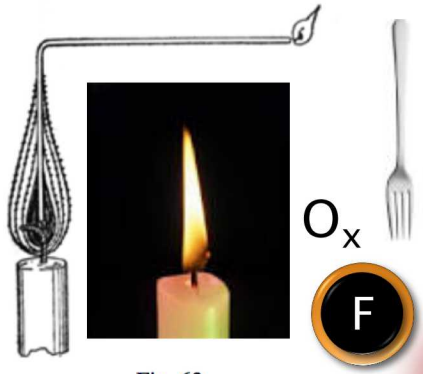

Fig. 62

"In the middle of the flame, where the wick is, there is this combustible vapor; on the outside of the flame is the air which we shall find necessary for the burning of the candle"

Q:

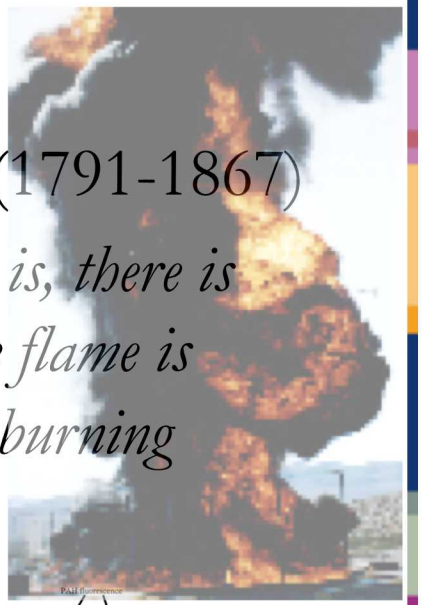

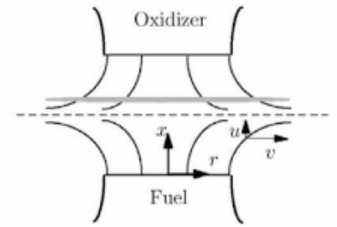

Figure 7. Schematic diagram of opposed-flow diffusion flame (adapted from Lutz et al., 1997).

FLAME facility

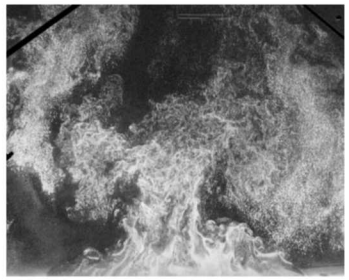

FIGURE 2. Sample raw PIV image in 1 m diameter helium plume (from Test 25).

O'Hern et al., JFM, 2005

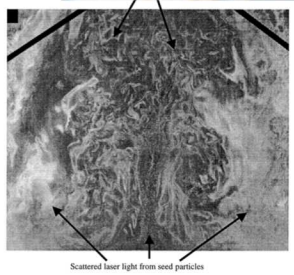

Tieszen et al., C&F 2002

Evolution of a Mindset: From Simple to Complex

- Peak radiative heat fluxes to engulfed objects is a function of fuel type, pool size, obstructions/accident geometry, and presence of cross-flow
- As cross-flow and geometric complexity of accident scenarios increase, SNL has found that transitioning from a Reynolds-Averaged Navier-Stokes (RANS) to a more predictive large-eddy simulation (LES) approach is required → HPC on Next-Gen platforms (NGP)

RANS-based → LES-based

Quiescent; q''_r
~ 100 kW/m^2

Cross-flow; q''_r
~ 200 kW/m^2

Whirls
>> 200 kW/m^2

Choice of Turbulence Modeling

- Direct Numerical Simulation (DNS), Large Eddy Simulation (LES) and Reynolds-Averaged Navier-Stokes (RANS) approaches define the computationally required time- and length scales
- Pool Fire Use-Case: large length and time scales challenge compute platforms
  - 1 cm resolution for a ten meter pool fire would require ~1 billion elements (only to a height of 1D)
  - 1 mm ~ 1 trillion elements (neglects bluff body requirements)

[1]

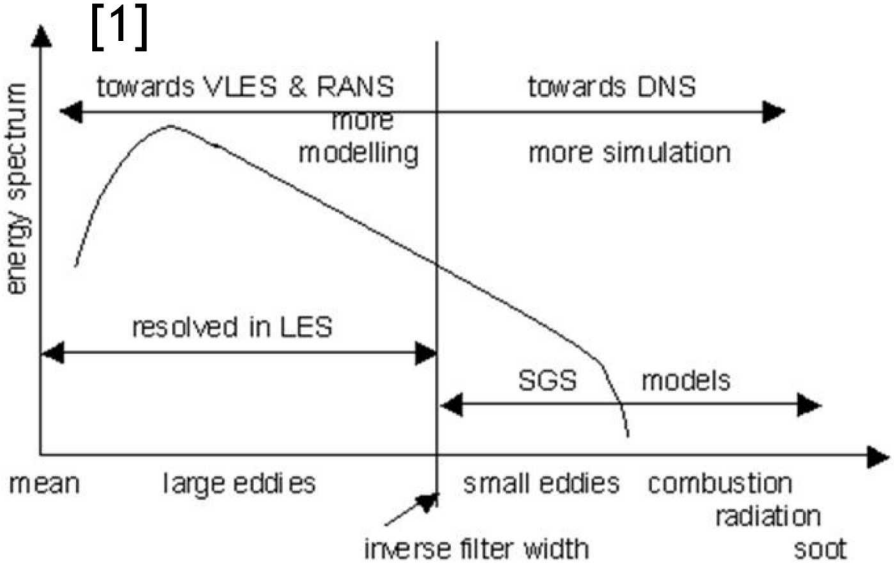

Direct Numerical Simulation:

- Simulation captures all relevant length- and time-scales
- No turbulence modeling
- Very expensive; total cost ~Re^3

Large Eddy Simulation

- Resolve the large-scale motion that contains most of the flow's energy
- Model small scale based on scale-similarity
- Model = f(D)

Reynolds-Averaged Navier-Stokes

- Model the turbulence spectrum
- Empirical in nature

[1] https://sites.google.com/site/smokeisnojoke/lesrans2.jpg

Fires/Plumes in Quiescent Conditions: The *classic* Abnormal/Thermal Environment (circa 1990)

- Quiescent pool fires are, essentially, large-scale diffusion flames, i.e., mixing limited non-premixed combustion
- Several instabilities dominate, including Rayleigh/Taylor (bubble spike, heavy on light fluid) and Kelvin Helmholtz (velocity shear between two streams)

Time-averaged (inset transient)

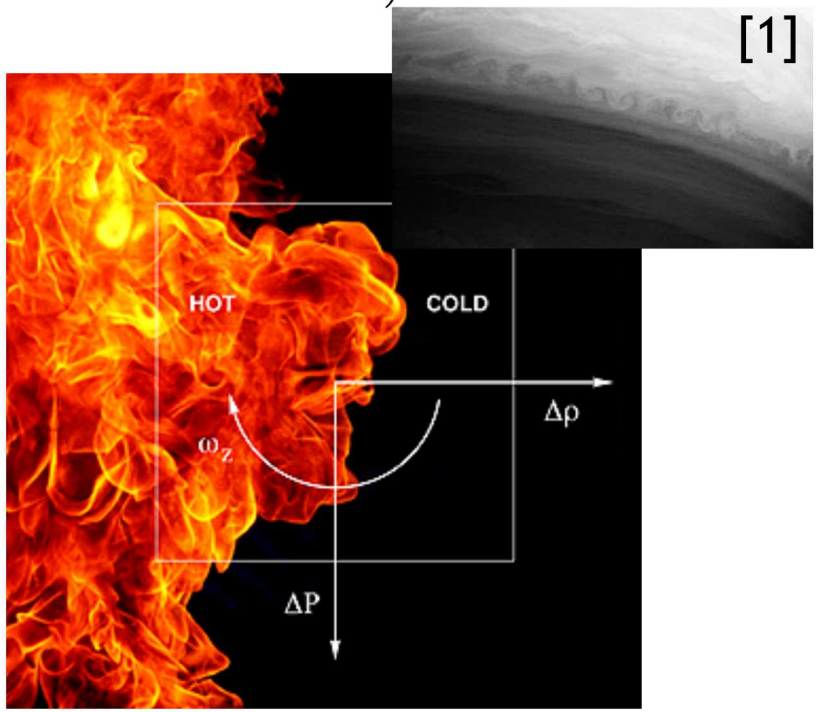

Vorticity generation (baroclinic torque), Rayleigh Taylor (RT) and Kelvin Helmholtz(KH) instabilities are present

[1] https://en.wikipedia.org/wiki/Kelvin-Helmholtz_instability

Quiescent Fire/Plume Physics

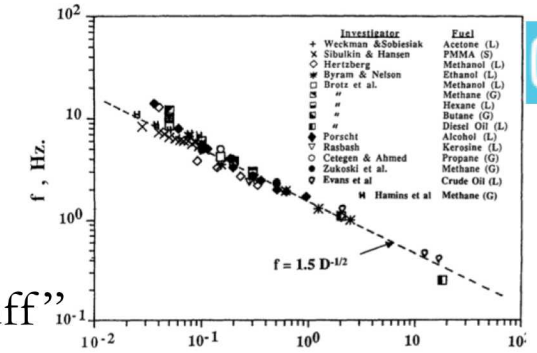

Cetegen and Ahmed, C&F 1993

- Fires, just as all buoyant plumes, in quiescent conditions "puff"
- In this application space, radiative heat transfer dominates

Hydrogen, Tieszen et al., *C&F,* 2004

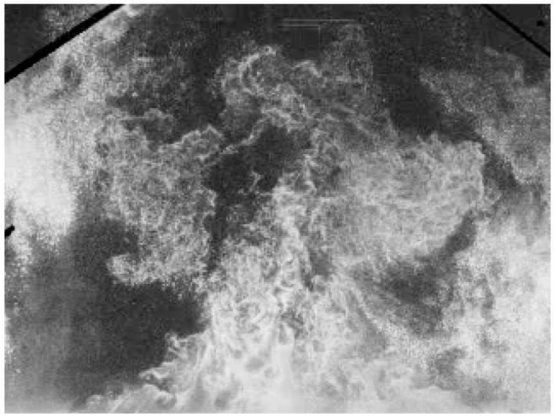

Helium, O'Hern et al., *JFM,* 2005

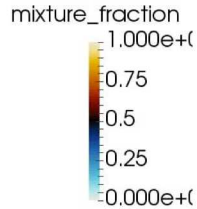

Helium DNS, Domino, (unpublished) 2016

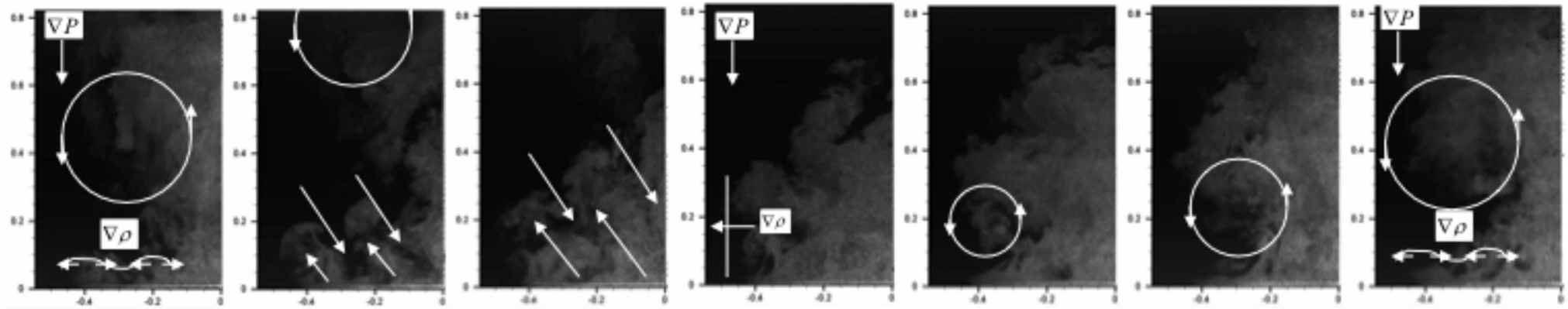

Evolution of a Puff Cycle (O'Hern et al., *JFM*, 2005)

Quiescent Fire/Plume Physics Convergence

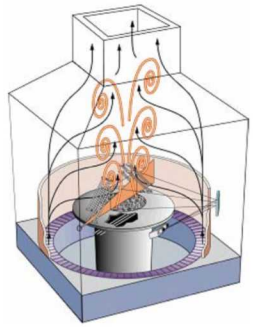

FLAME Facility

- Solution Verification, i.e., mesh-independent results can be challenging
- Sandia's FLAME facility and experimental pedestal design drives dip in centerline vertical velocity (aleatory and epistemic uncertainty)
- Turbulence modeling shown herein has no modeled term for production of turbulent kinetic energy due to buoyancy
- Therefore, core collapse is predicted only when small-scale RT and KH instabilities are resolved (sub-centimeter scale)

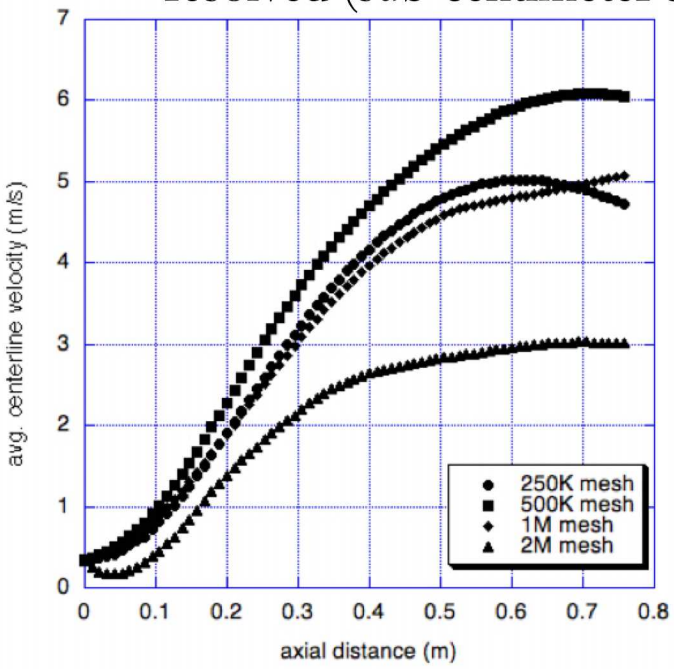

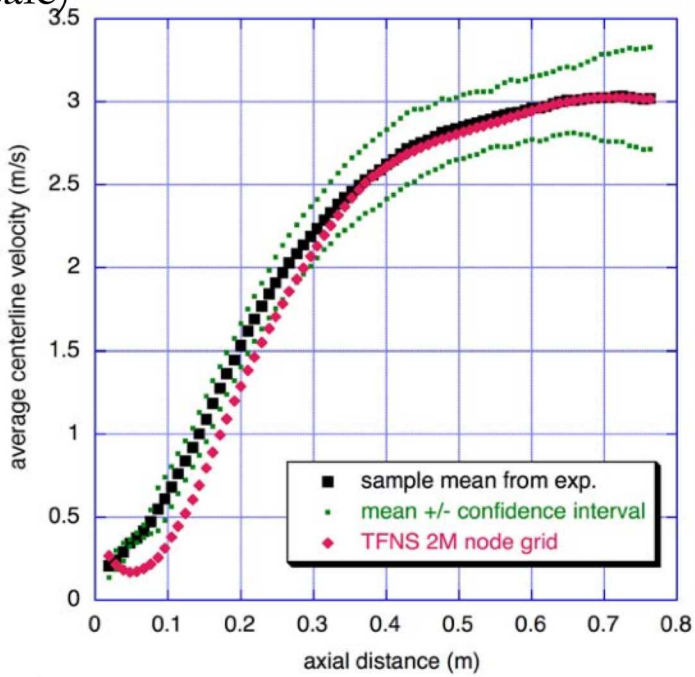

Tieszen, Domino, and Black, *SAND*, 2005

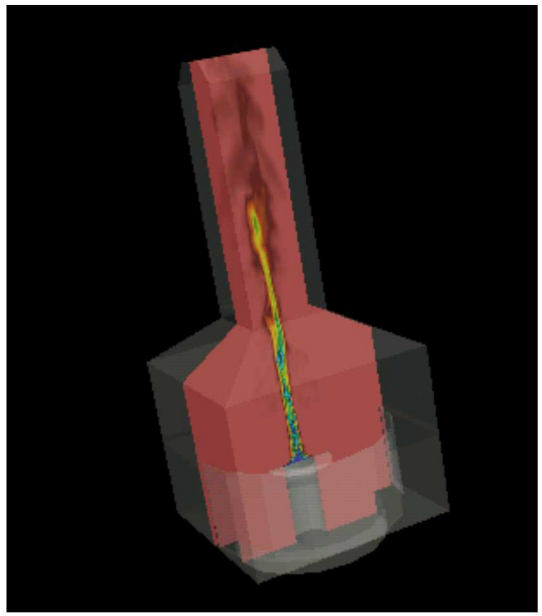

Computational Domain

LES-based Solution Verification (Brown, et al., *SAND*, 2017)

- Increasing mesh resolution captures core collapse and flame/entrainment fingering

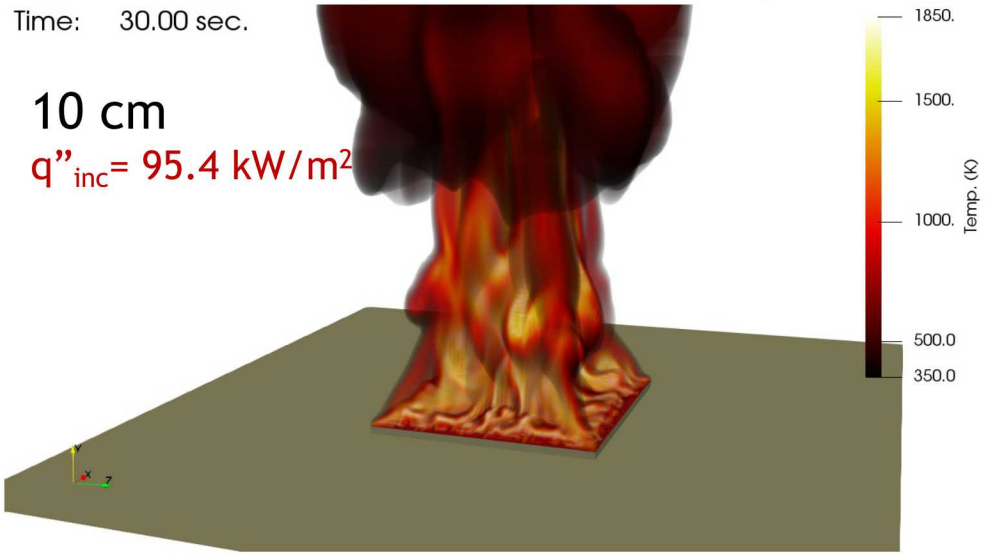

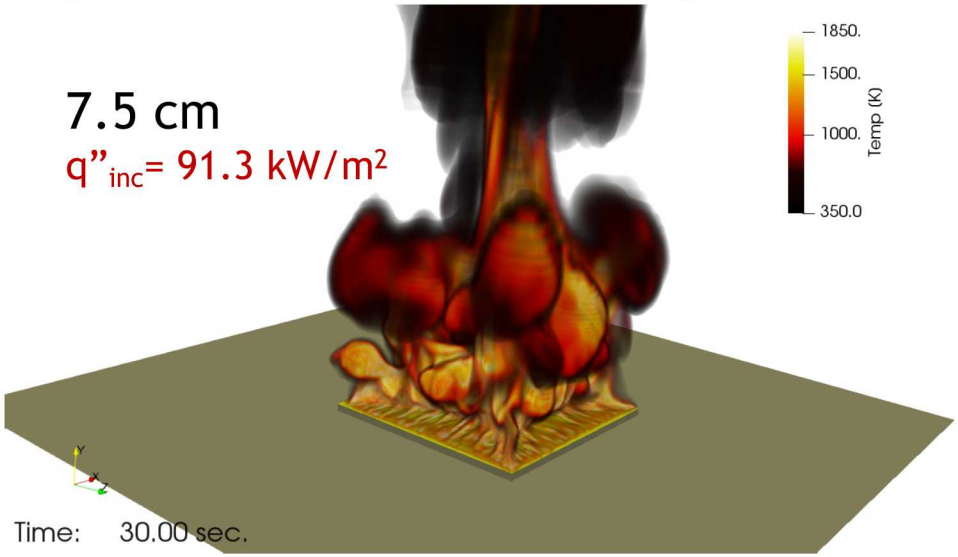

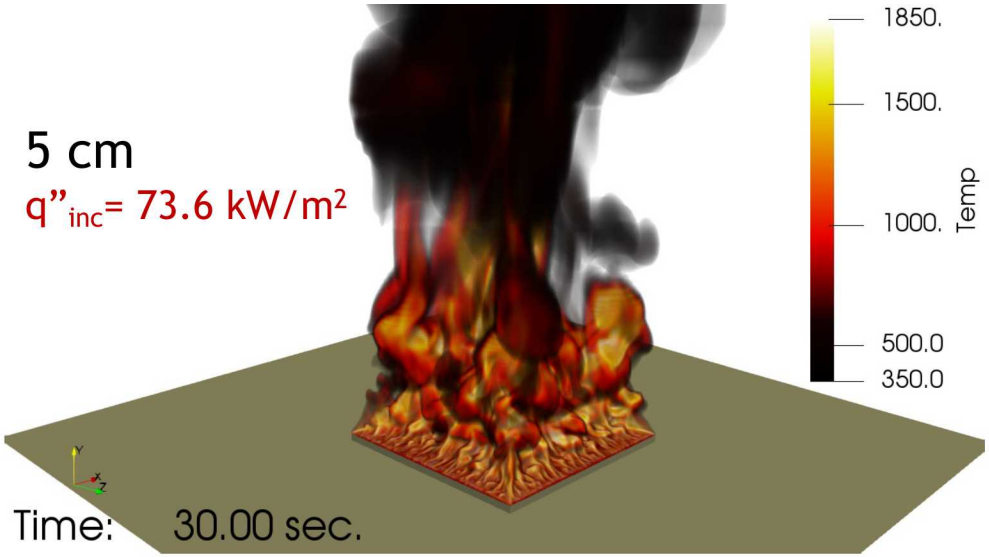

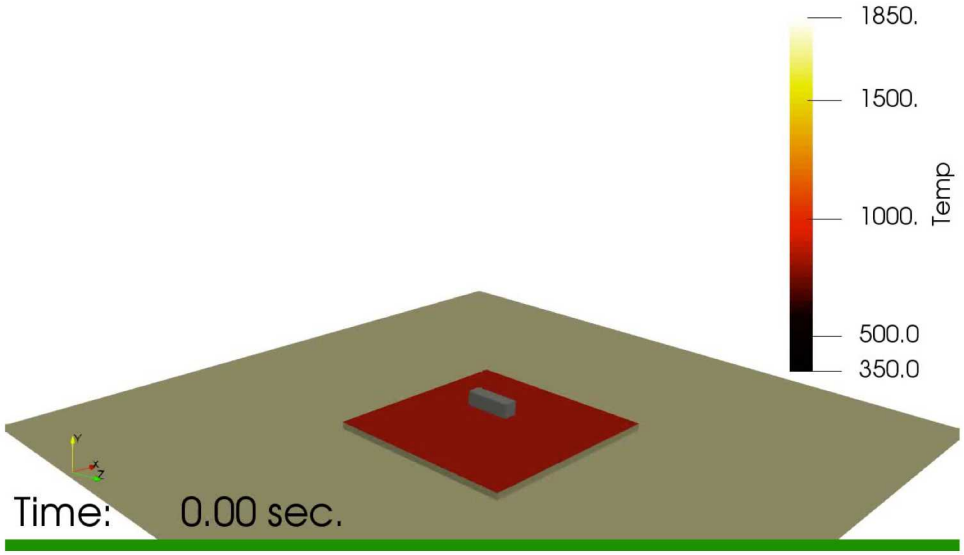

Evolution of a Mindset….. Crossflow

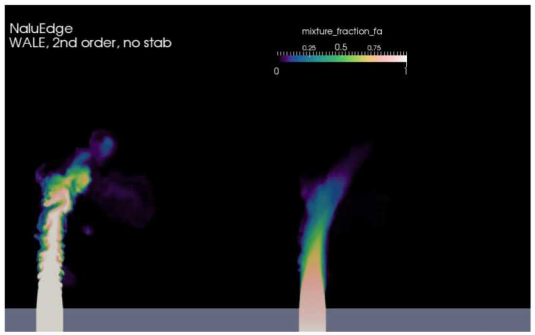

LES-based Su and Mungal (Re 5000) simulation (mixture fraction shading)

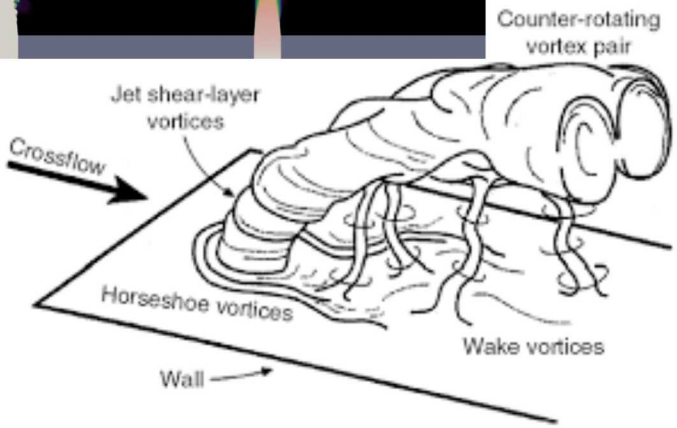

Fric and Roshco, *JFM*, 1994

- ***Finding***: The inclusion of a crossflow wind profile couples vorticity of the pool and streamwise momentum that drives the formation of column vortices, increases the importance of mixing and, therefore, convective loads on the object become more important
- ***Change in mindset***: Invest in validation use cases to highlight the importance of fire accident scenarios in the presence of crossflow

Ten meter (top) experiment (Nakos) and three meter (bottom) simulation (Domino and Tieszen)

Turbulence Modeling in the Presence of Mixed Convection

- Model Configuration: SNL-based Sean Kearney Experiment, "Experimental investigation of a cylinder in turbulent convection with an imposed shear flow", *AIAA*, 2005
- Present day RANS Conclusion: The presence of the heated bottom wall significantly challenged ability to predict the QoI (normal heat flux to cylinder)

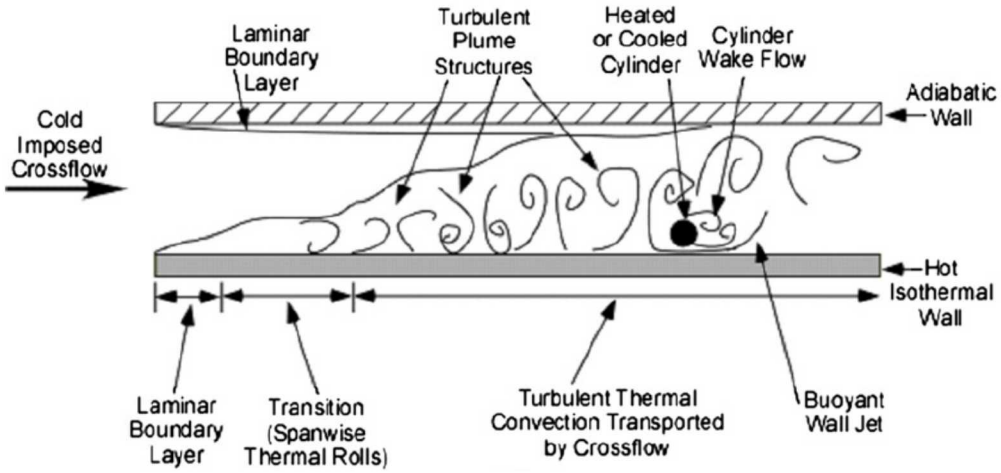

Kearney experimental configuration

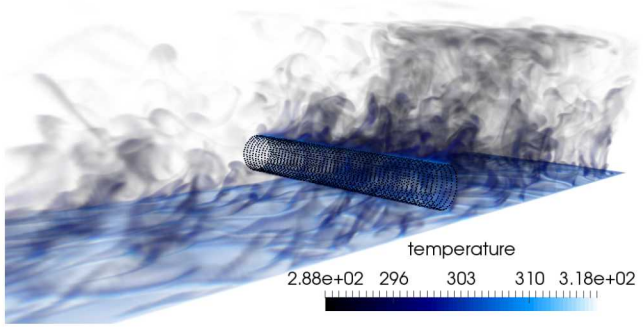

Domino et al., *CTRSP*, 2016

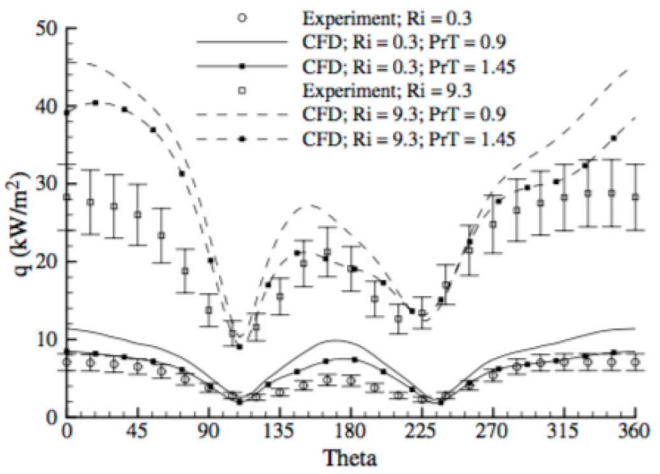

Fig. 13. Effect of turbulent Prandtl number on cylinder heat flux predictions for cases 3 (cooled cylinder) and 4 (heated cylinder).

Laskowski et al., *AIAA*, 2007

RANS-based simulation (v2-f, k-e) study conducted by Laskowski et al., *AIAA*, 2007

Research Thrust: High-quality LES-Based VVUQ Process

Established a sound LES-based verification and validation process (with uncertainty quantification) that includes the following attributes:

- Definition of key physics, Phenomena Identification Ranking Table (PIRT)
- Code implementation and verification
  - Including higher-order unstructured
- Validation including solution verification (meshes with converged statistics)
- Structural uncertainty, i.e., model form, quantification

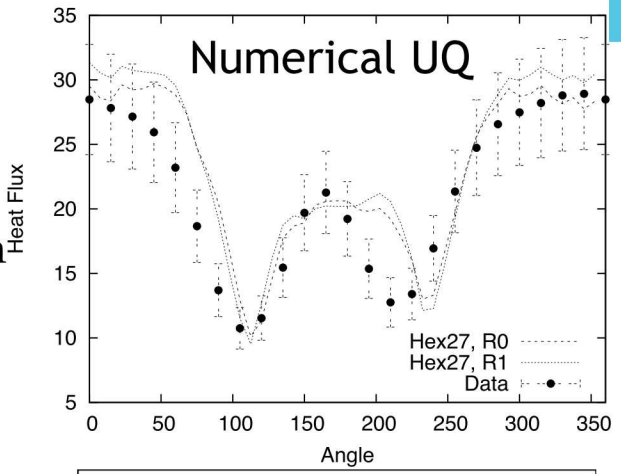

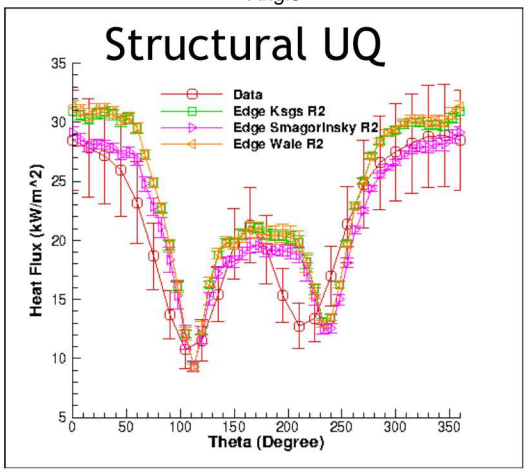

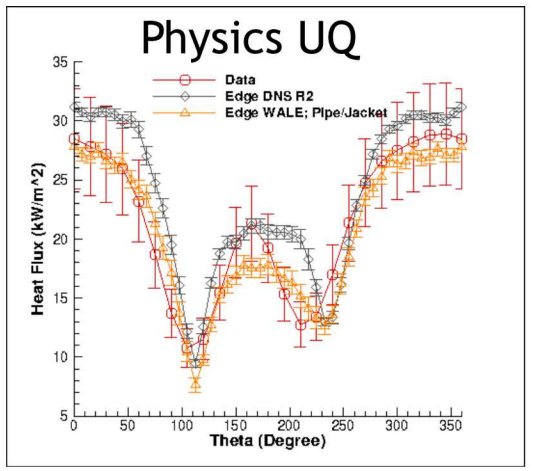

Non-isothermal MMS

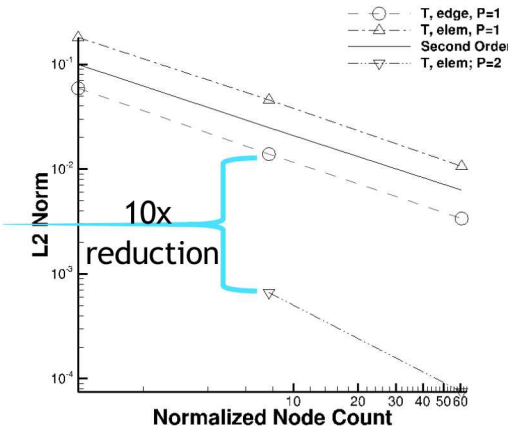

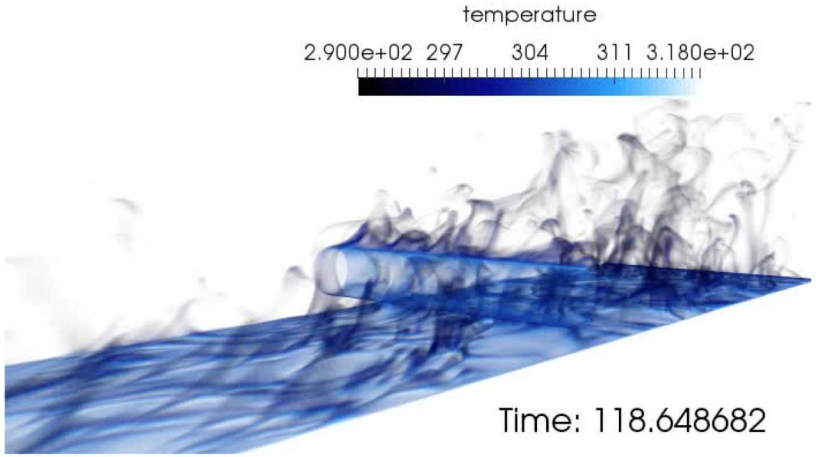

"An assessment of atypical mesh topologies for low-Mach LES", Domino et al., *Comp & Fluids*, 2019)

Research Thrust: Improved VVUQ: Automatic Structural Uncertainty

- Previous LES validation studies, e.g., cylinder in x-flow, three models were implemented and tested (verified and maintained in the code repository)
- Is there a more efficient approach? Yes! Eigenvalue perturbation of the SGS stress (extension of RANS-based approach: Emory et al., *Phys. Fluids*, 2017)

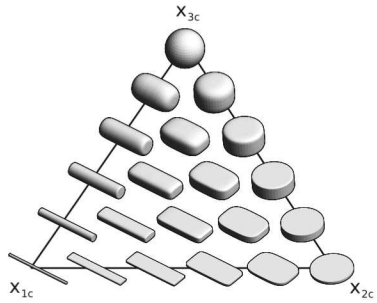

Barycentric triangle (see Lumley and Newman, *J. Fluid Mech.*, 1977)

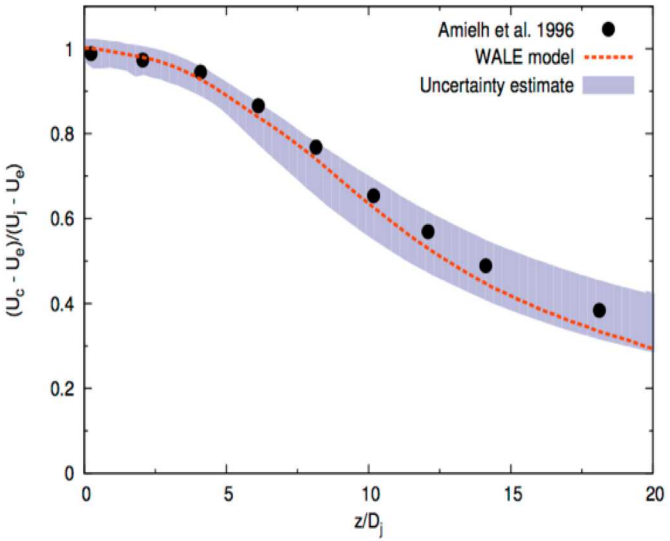

$$\tau_{ij}^{sgs} - \frac{\tau_{kk}^{sgs}}{3}\delta_{ij} = -2\nu_{sgs}\overline{S}_{ij},$$

$$a_{ij}^{res} = \frac{1}{\overline{u_k u_k}}\left(\overline{u}_i\overline{u}_j - \frac{\overline{u}_k\overline{u}_k}{3}\delta_{ij}\right) = v_{in}^{res}\Lambda_{nl}^{res}v_{jl}^{res}$$

$$a_{ij}^{sgs} = \frac{1}{\overline{u_k u_k}}\left(\tau_{ij}^{sgs} - \frac{\tau_{kk}^{sgs}}{3}\delta_{ij}\right) = v_{in}^{sgs}\Lambda_{nl}^{sgs}v_{jl}^{sgs},$$

$$\overline{u_i u_j}^{*} = \overline{u}_i\overline{u}_j + \tau_{ij}^{sgs*} = \overline{u}_i\overline{u}_j + \overline{u_k u_k}^{*}a_{ij}^{sgs*} + \frac{\tau_{kk}^{sgs*}}{3}\delta_{ij},$$

$$\overline{u_k u_k}^{*} = \overline{u}_k\overline{u}_k + \tau_{kk}^{sgs*} \quad \text{and} \quad a_{ij}^{sgs*} = v_{in}^{sgs*}\Lambda_{nl}^{sgs*}v_{jl}^{sgs*}.$$

Open jet

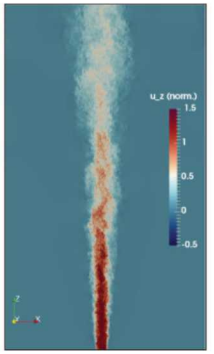

- Jofre, Domino, and Iaccarino, *Flow Turb. Comb*, 2018 (plane turbulent channel)
- Jofre, Domino, and Iaccarino, *Int. J. Heat & Fluid Flow*, 2019 (turbulent axisymmetric jet)

Research Thrust: Large-Scale Fire Dynamics in the Presence of Cross Flow

- The coupling of crosswind with a hydrocarbon fire event drives large-scale column vortex formation – very similar to classic jet-in-cross flow behavior
- Increased mixing yields increased radiative heat fluxes
- Although benchscale efforts exist for quantities such as flame drag distance and tilt angles, none exist for this scale of interest, e.g., 10 meters and beyond
- We (Domino and Scott, 2020 ASC V&V) are quantifying large-scale fire physics (Γ, θ, etc.) through theory (Mahesh, *Annual Rev. Fluid Mech*, 2013) and simulation (LES-based)
- Wake vortices have ***never*** been realized in simulation (ABL/CVP interactions)
- Deploy automatic LES-UQ methodology
  - Proposed CTRSP 2020

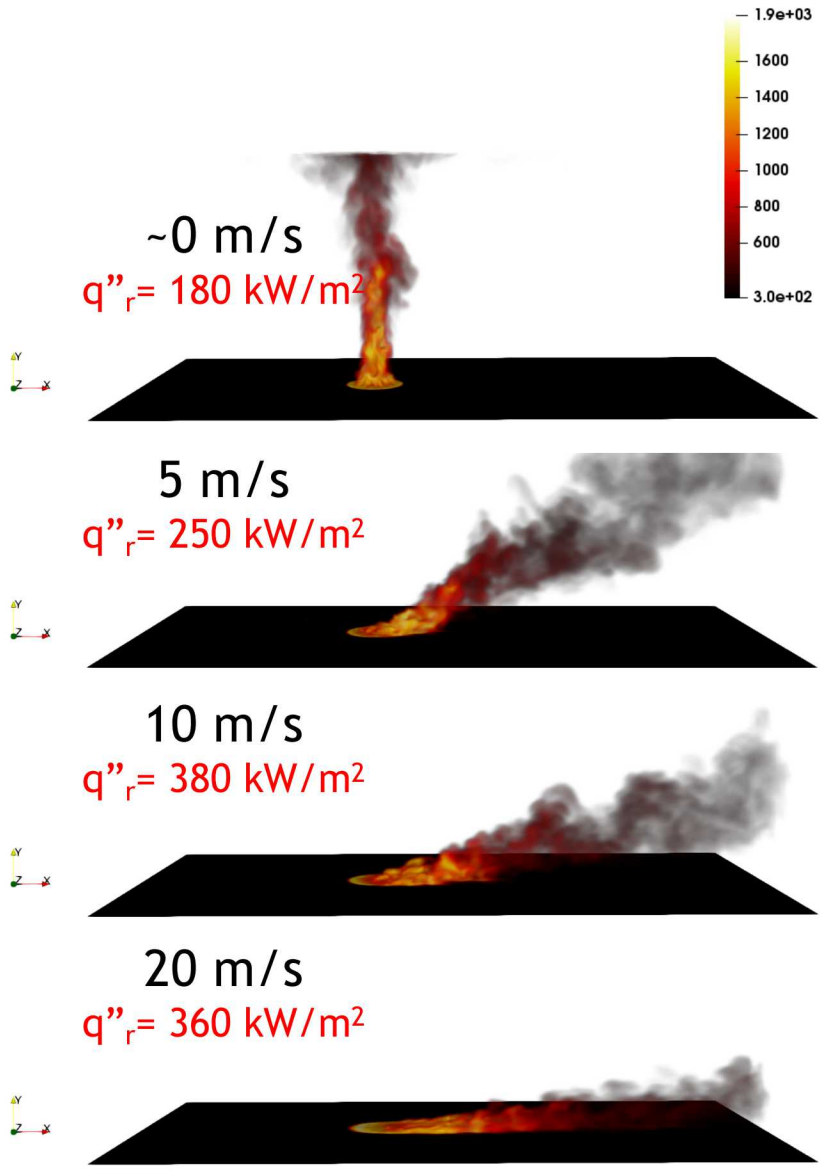

10 m pool fire
LES-based numerical study with varying cross wind

Evolution of a Mindset…..Whirling-like Flow

- Fire whirls significantly increase pear radiative and convection loads to due increased mixing rate (>>200 kW/m^2)
- Phenomena can be rather common in real scenarios (see Fig 3 of Tohidi et al., *Annual Rev. Fluid Mech.*, 2018), e.g., L-s, hills, etc.

Brush fire (Curtin Springs, Australia)

Fig. 19. Formation of a fire whirl during field experiments at Gestosa.

Pinto et al., *Fire Safety J.*, 2017

Fire whirls from a 3-meter diameter pool in the Fire Laboratory for Accreditation of Modeling by Experiment, or FLAME, facility at Sandia National Laboratories.
(Photo by Richard Simpson; A. Hanlin, lead experimentalist)

Research Thrust:
LES-based Modeling Whirling-like Flow

- Idealized chamber in which swirl is provided by selective wall placement (clockwise)
- Buoyant (vertical) acceleration induces tangential entrainment, and, hence, internal circulation (Pinto et al., *Fire Safety J.*, 2017)
- Gap, g, varied between 10, 20, and 40 cm
  - Pinto et al, g = 10 cm, height = 6m)

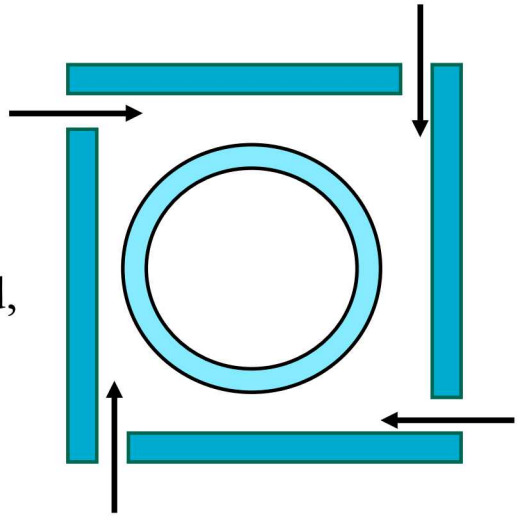

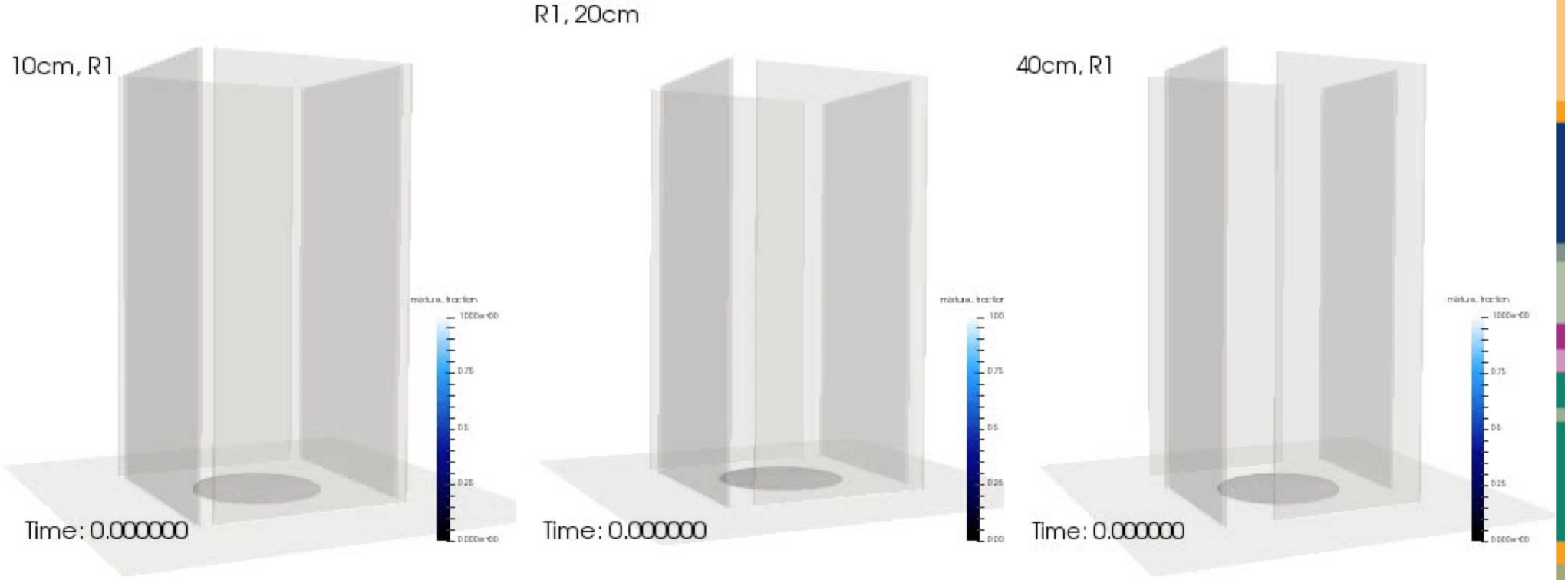

Volume rendered mixture fraction

Low-Mach Turbulent Reacting Flow Equation Set

- Favre-averaged, variable-density, low-Mach equation set using large-eddy simulation (LES)
  - Acoustics are filtered via the low-Mach derivation (Rehm and Baum, 1978; Paolucci, 1982)

$$\int \frac{\partial \bar{\rho}}{\partial t}\, dV + \int \bar{\rho}\tilde{u}_j n_j\, dS = 0$$

Given filter: $\overline{\phi(\boldsymbol{x},t)} \equiv \int_{-\infty}^{+\infty} \phi(\boldsymbol{x}',t) G(\boldsymbol{x}'-\boldsymbol{x})\, \mathrm{d}\boldsymbol{x}'$

$$\int \frac{\partial \bar{\rho}\tilde{u}_i}{\partial t}\mathrm{d}V + \int \bar{\rho}\tilde{u}_i\tilde{u}_j n_j \mathrm{d}S = \int \tilde{\sigma}_{ij} n_j \mathrm{d}S - \int \tau_{ij}^{sgs} n_j \mathrm{d}S + \int \left(\bar{\rho}-\rho_\circ\right) g_i \mathrm{d}V$$

$$\int \frac{\partial \bar{\rho}\tilde{h}}{\partial t}\mathrm{d}V + \int \bar{\rho}\tilde{h}\tilde{u}_j n_j \mathrm{d}S = - \int \bar{q}_j n_j \mathrm{d}S - \int \tau_{h,j}^{sgs} n_j \mathrm{d}S - \int \frac{\partial \bar{q}_i^r}{\partial x_i}\mathrm{d}V + \int \left(\frac{\partial \bar{P}}{\partial t} + \tilde{u}_j \frac{\partial \bar{P}}{\partial x_j}\right) \mathrm{d}V + \int \overline{\tau_{ij}\frac{\partial u_i}{\partial x_j}}\mathrm{d}V$$

Subgrid Stress (SGS):

$$\tau_{ij}^{sgs} \equiv \bar{\rho}(\widetilde{u_i u_j} - \tilde{u}_i\tilde{u}_j)$$
$$\tau_{h,j}^{sgs} \equiv \bar{\rho}\left(\widetilde{hu_j} - \tilde{h}\tilde{u}_j\right)$$
$$\tau_{Z,j}^{sgs} \equiv \bar{\rho}\left(\widetilde{Zu_j} - \tilde{Z}\tilde{u}_j\right)$$

$$\int \frac{\partial \bar{\rho}\tilde{Z}}{\partial t}\mathrm{d}V + \int \bar{\rho}\tilde{u}_j\tilde{Z} n_j \mathrm{d}S = - \int \tau_{Z,j}^{sgs} n_j \mathrm{d}S + \int \bar{\rho} D \frac{\partial \tilde{Z}}{\partial x_j} n_j \mathrm{d}S$$

Closure:

$$\tau_{ij}^{sgs} - \frac{1}{3}\delta_{ij}\tau_{kk}^{sgs} = -2\mu^t S_{ij}^*$$

$$\tau_{h,j}^{sgs} = -\frac{\mu_t}{\mathrm{Pr}_t}\frac{\partial \tilde{h}}{\partial x_j}$$

$$\tau_{Z,j}^{sgs} = -\bar{\rho} D_t \frac{\partial Z}{\partial x_j}$$

LES Models:

Smagorinsky: $\mu_t = \rho\left(C_s\Delta\right)^2 |\tilde{S}|$

Ksgs: $\mu_t = C_{\mu_\epsilon}\Delta k^{\mathrm{sgs}\,\frac{1}{2}}$

WALE: $\mu_t = \rho\left(C_w\Delta\right)^2 \dfrac{\left(S_{ij}^d S_{ij}^d\right)^{3/2}}{\left(S_{ij}S_{ij}\right)^{5/2} + \left(S_{ij}^d S_{ij}^d\right)^{5/4}}$

- mixture fraction-based flamelet combustion with generalized heat loss (multi-D table look-up)
- Soot: Koo et al. (2018) from Moss and Askit (2007)

Thermal Radiation Technique: Discrete Ordinate Method (DOM)

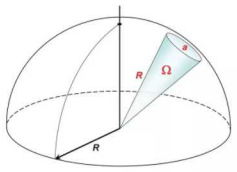

Definitions:

I^k = Intensity for ordinate k

s^k_j = ordinate k for direction j

w = test function

N = quadrature set, e.g., 2, 4, 6, .., 12

- Radiative Transport Equation (RTE) approach attributes:
  - Requires discretization, stabilization, quadrature set, T^g, μ_a, μ_s, etc.
  - A meshed interior "volume"; Note: $\varepsilon = f(\Delta x^n, N)$
- Large set of sparse linear solves ~ $8N^2$ (Thurgood); N ~ 4
- Path forward: conservative Streamwise Upwind Control Volume (SUCV) stabilization motivated by SUPG Burns et al.., *Ntl. Heat Trans Conf.*, 1995, provided by Domino, *SAND*, 2014

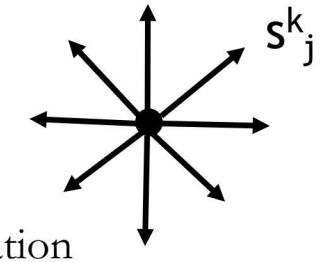

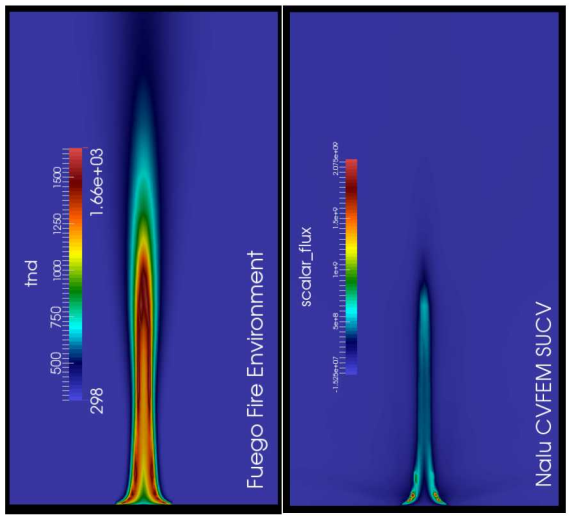

5 meter JP-8 Pool Fire
temperature and absorption coeff

$$s_j^k \frac{\partial I^k}{\partial x_j} + (\mu_a + \mu_s)\, I^k = \frac{\mu_a \sigma T^4}{\pi} +$$

$$\int \tilde{w} \left(s_j^k \frac{\partial I^k}{\partial x_j} + (\mu_a + \mu_s)\, I^k - \left(\frac{\mu_a \sigma T^4}{\pi} + \frac{\mu_s G}{4\pi} \right) \right) dV = 0$$

$$\int s_j^k I^k n_j dS + \int \left((\mu_a + \mu_s)\, I^k - S \right) dV = \int \tau s_j^k R^k n_j dS$$

$$G \approx \sum_k w_k I^k \qquad \tilde{w} = w + \tau \left(s_j \frac{\partial}{\partial x_j} w + \alpha \mu_a w \right)$$

RTE with isotropic scattering

Thermal (heat conduction) and multi-physics coupling

- The quantity of interest is generally thermal response, $T = f(t,x_i)$, and incident radiative flux, H

Thermal Equation (simple):

$$\rho C_p \frac{\partial T}{\partial t} - \frac{\partial}{\partial x_j}\lambda\frac{\partial T}{\partial x_j} = 0$$

Thermal interface coupling:

$$q_n = -\lambda\frac{\partial T^s}{\partial x_j}n_j^s = \varepsilon[\sigma T^4 - H] + h(T - T^\infty)$$

Fluids/PMR coupling:

$$\frac{\partial q_j^R}{\partial x_j} = \mu_a[4\sigma T^4 - G]$$

Intensity coupling:

$$I = \frac{1}{\pi}[\tau\sigma T_e^4 + \varepsilon\sigma T^4 + \rho H]$$

From fluids: T, μ_a, μ_s

Supplemental:

$$H \approx \sum_{n_j s_j^k > 0} w_k I^k |n_j s_j^k| \qquad G \approx \sum_k w_k I^k$$

Three-Way Reacting Flow (Fire Mechanics) Coupling Description

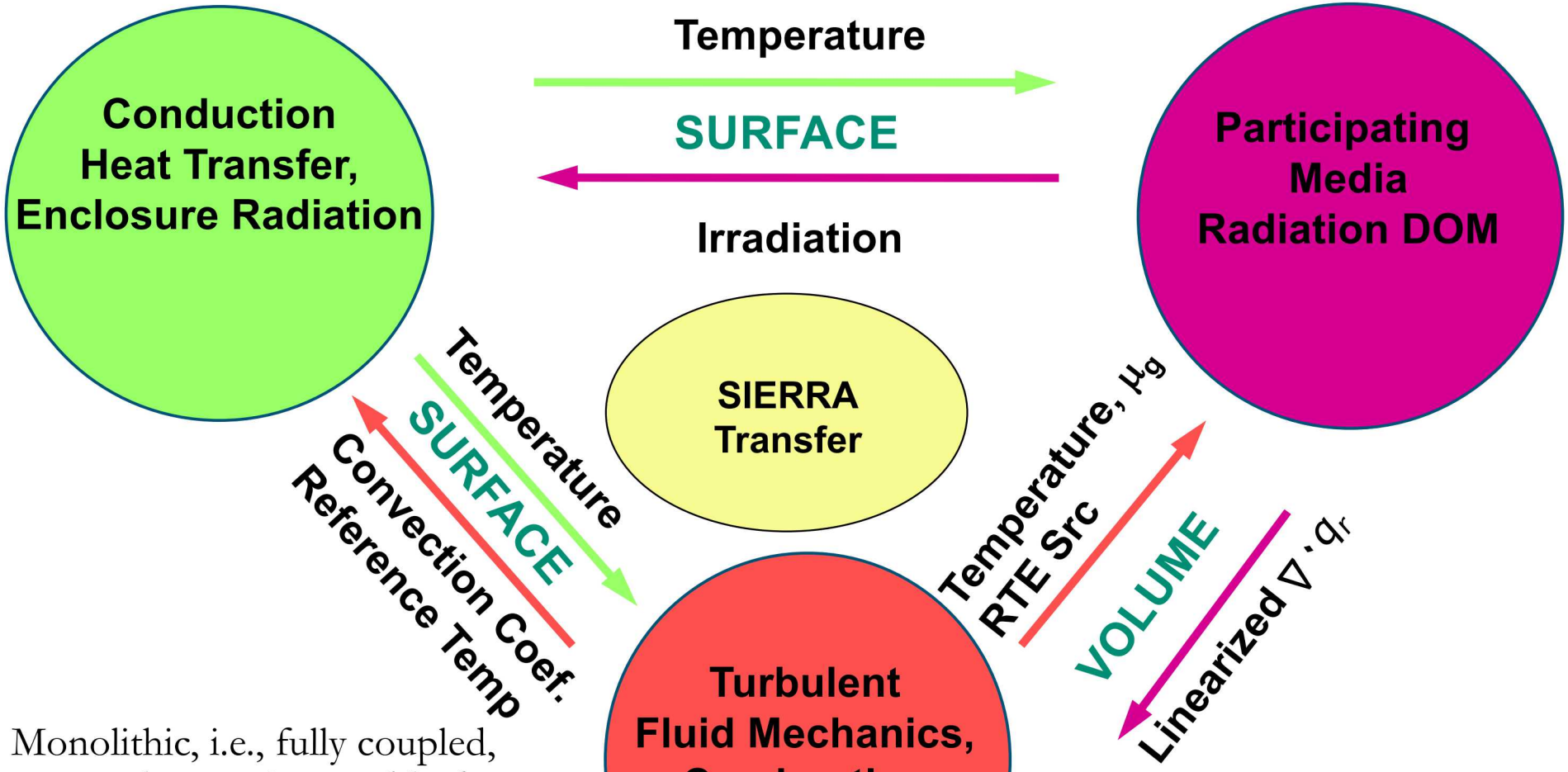

- Monolithic, i.e., fully coupled, approaches are intractable due to the size of $(u, v, w, p, h, h^r, Z, I^k\ T)^T$
- Stable and accurate operator split methods are, therefore, sought
  - See Domino et al., *AIAA*, 2007

Example of Multi-Physics Operator Split Methods

Conduction Heat Transfer, Enclosure Radiation

- Compute amplification factor: $T^{n+1} = \lambda T^n$ Require: $|\lambda| \leq 1$
- CHT via flux transfer:
  - Unstable for certain Δt and material property ratios
- CHT via convection coefficient:
  - Unconditionally stable, however, Δt erro

Temperature

SURFACE

Convection Coef.

Reference Temp

Turbulent Fluid Mechanics, Combustion

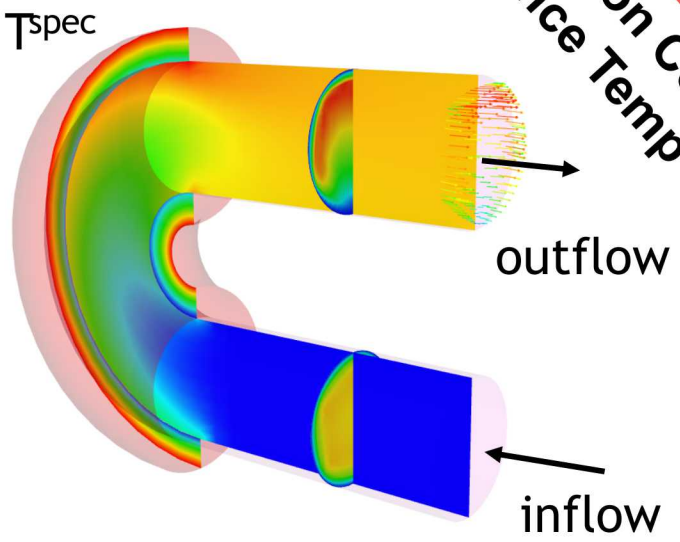

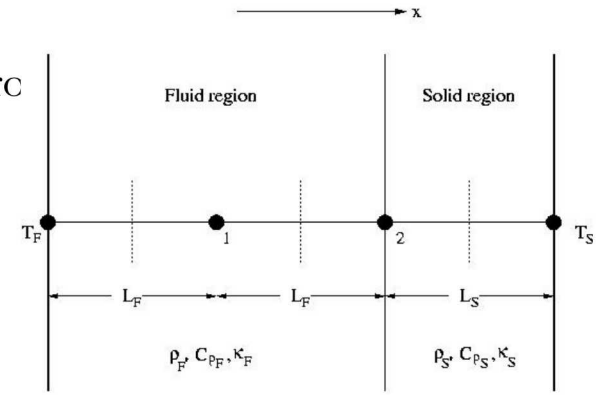

Simplified 1D geometry with 2 nodes for stability analysis of CHT

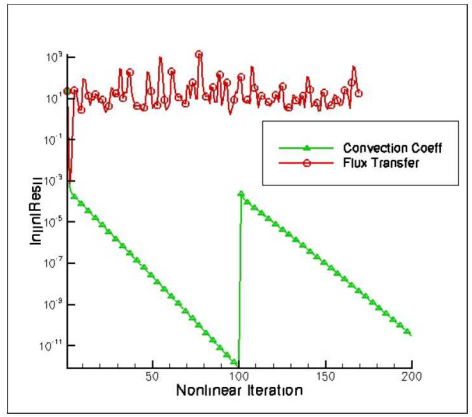

low-Mach Codes Featured

- Nalu Philosophy:
  - Open-source BSD-clause 3

https://github.com/NaluCFD

- Sierra/Fuego Philosophy:
  - Government use license or Cooperative R&D Agreement (CRADA)

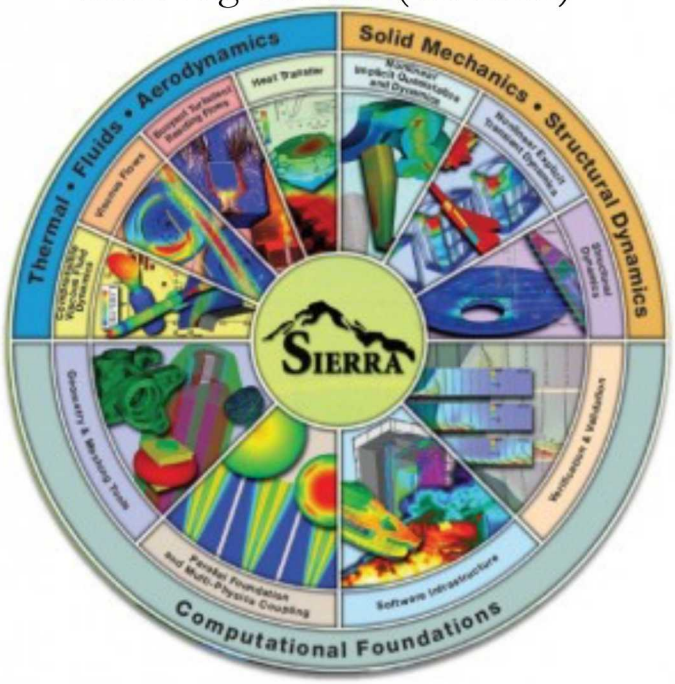

ASC™ (soon)

Reality: Meshing time for complex applications remains a significant bottleneck!

- Many applications of interest include complex geometries
- low-Mach fluids users interested in high-quality simulation results tend towards hexahedral-based topologies (if possible)
- However, if a scheme is "design-order" accurate, and low-dissipation, any topology may suffice
  - Cast this in terms of *efficiency* (not unlike the active discussion on low- vs higher-order)
- Sometimes, the penetration of a low-Mach fluids physics addition for a given analysis is high as the meshing can be prohibitively complex and time consuming, O(months)
- Research Thrust: Establish numerical accuracy/stability on generalized unstructured mesh topologies and deploy this methodology to conform to a fast-meshing architype
  - Likely tetrahedral-, or Voronoi-based, see Bres et al., AIAA 2018-3302, 2018)

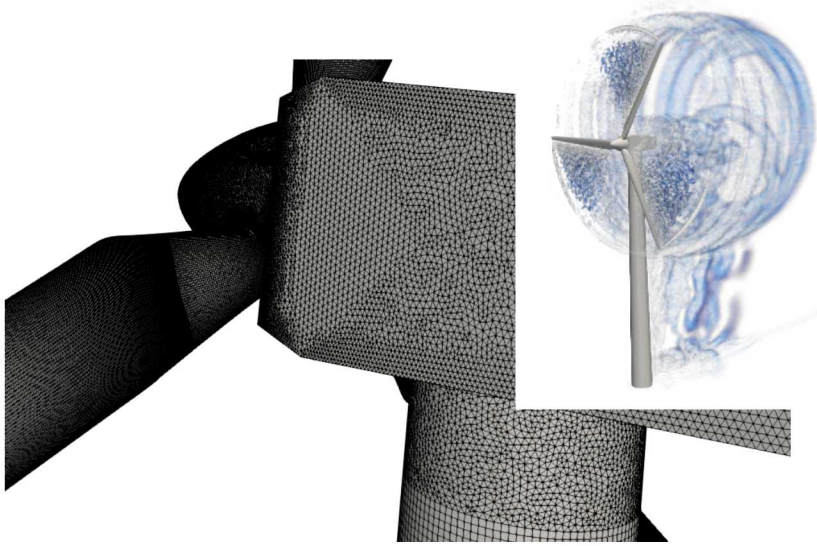

UUR Example: Vestas V27 225 kw
Hybrid low-order hex/tet/pyr/wedge

Sample of a somewhat complex geometry

A Review of a Typical V&V Workflow

- Verify on ***nice*** Hexahedral-based elements

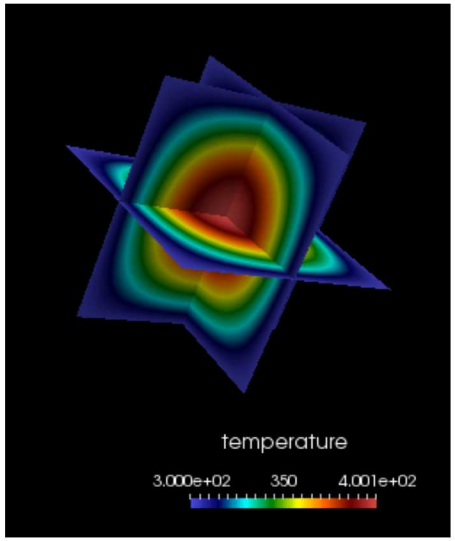

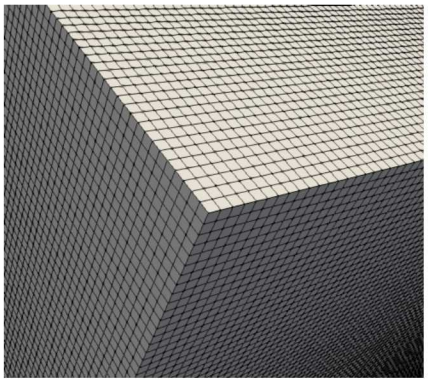

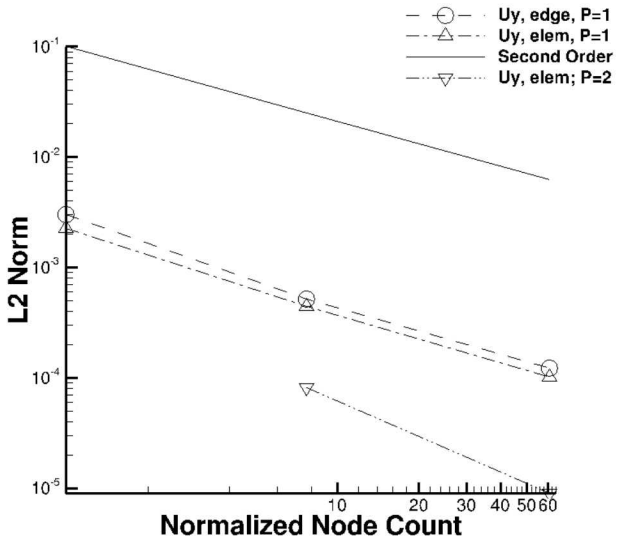

Variable-density low-Mach MMS (Domino, *CTRSP*, 2016)

- Validate on ***perfect*** meshes on a variety of canonical flows

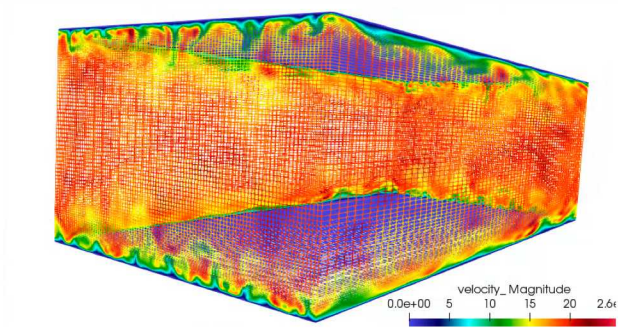

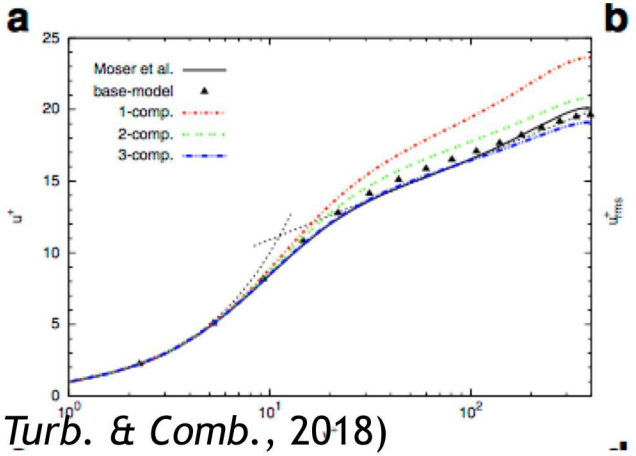

Re_τ 395 plain-channel (Jofre, Domino, Iaccarino, *Flow, Turb. & Comb.*, 2018)

Paradigm Shift for Numerical Methods Development: Meshing Bottleneck Drives Deployed Methods (Research Thrust)

- Verify on ***awful*** hybrid mesh element quality

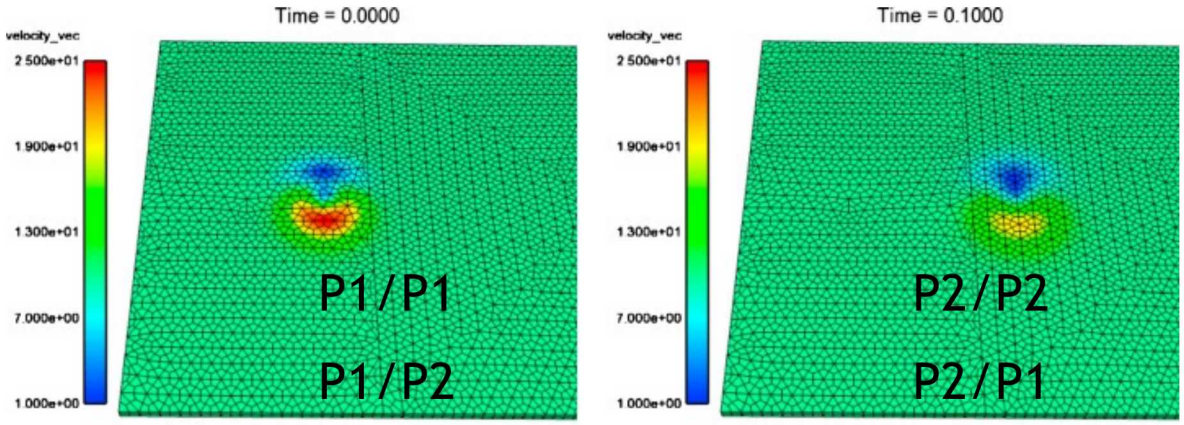

(a) Time = 0.0 seconds.

(b) Time = 0.10 seconds.

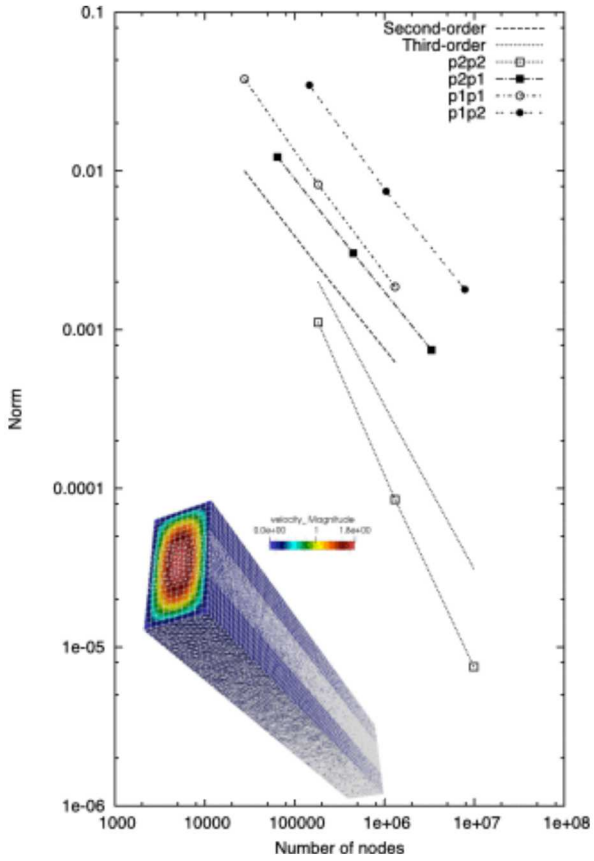

- Validate on ***non-ideal*** meshes on a variety of canonical flows

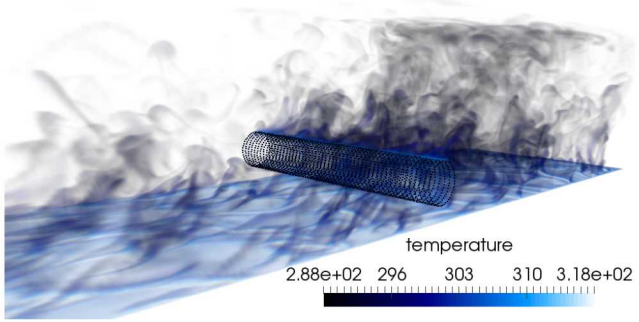

Chosen Discretization: Control-Volume Finite Element Method (CVFEM)

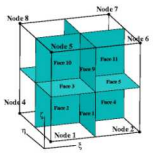

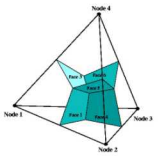

- A combination between the edge-based vertex-centered and FEM is the method known as Control Volume Finite Element (CVFEM)
- A dual mesh is constructed to obtain flux and volume quadrature locations
- As with FEM, a basis is defined:

$$T(x_k) \approx \sum_{i=1}^{npe} N_i(x_k) T_i \qquad \frac{\partial T(x_k)}{\partial x_j} \approx \sum_{i=1}^{npe} \frac{\partial N_i(x_k)}{\partial x_j} T_i$$

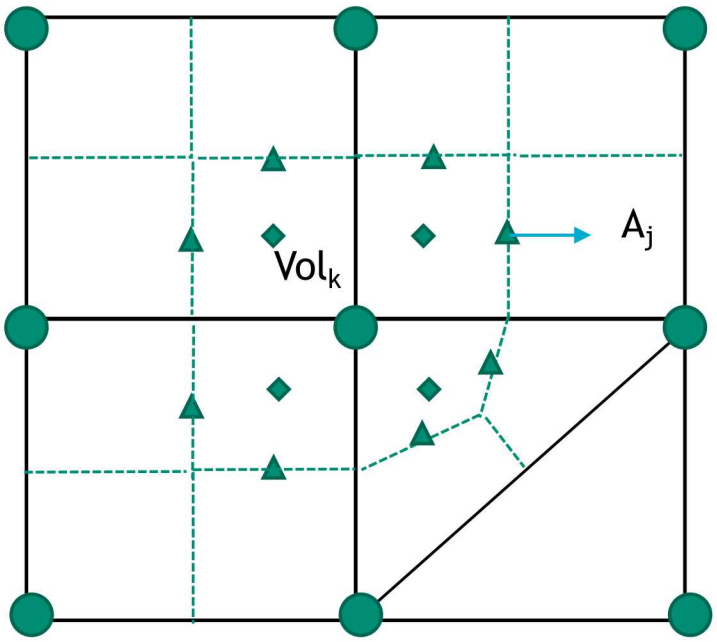

dual-volume definition

- Edge-based assembles A_j and Vol_k to edges and nodes, respectively

- Integration-by-parts over test function w:

$$\int w\rho C_p \frac{\partial T}{\partial t} dV + \int \frac{\partial w}{\partial x_j} \lambda \frac{\partial T}{\partial x_j} dV - \int w\, \lambda \frac{\partial T}{\partial x_j} n_j dS = 0$$

- However, define a test function, w, as a piece-wise constant function (Heaviside) to be 1 inside the dual volume and 0 outside. Gradient is a Dirac-delta function:

$$\frac{\partial w}{\partial x_j} = -n_j \delta(x_j - x^{IP}{}_j)$$

- Leading to:

$$\int \rho C_p \frac{\partial T}{\partial t} dV - \int \lambda \frac{\partial T}{\partial x_j} n_j\, dS = 0$$

Control-Volume Finite Element Method Attributes

- CVFEM can be viewed as Petrov-Galerkin method
- The method can also be promoted in polynomial space, see Domino, *CTRSP*, 2014 as a first example of low-Mach fluids algorithm – or Domino, *JCP*, 2018
- Possible higher efficiency on NGP due to increased local work)
- However, suitability of higher-order for LES is an open argument – especially when other errors/uncertainties exist

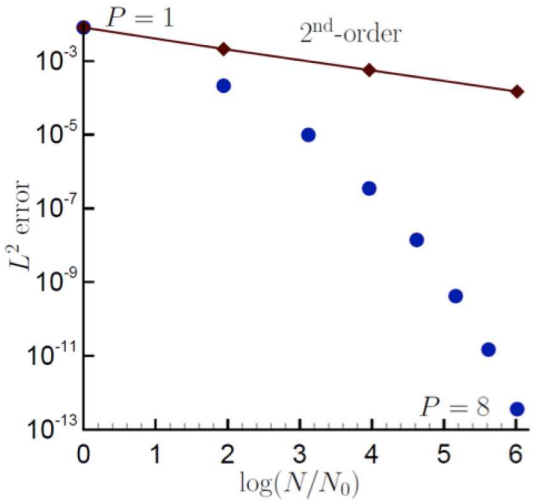

Spectral convergence

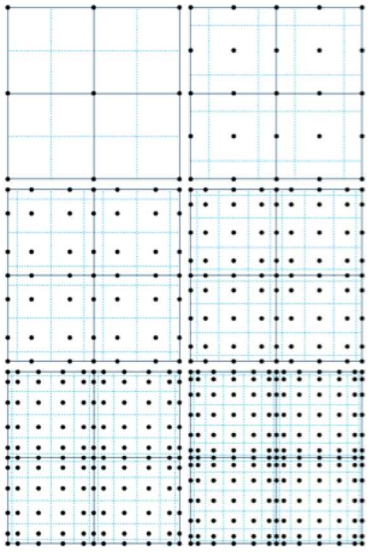

Dual-volume for promoted quad4

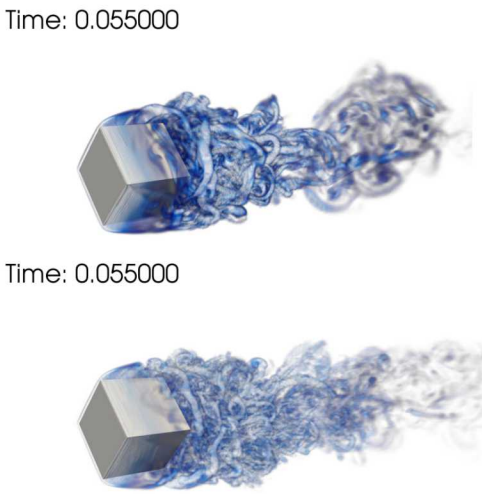

Rotating cube (Re 4000, RPM 3600)
P=1 (top) and P=2 (bottom)

P=1 (left) and P=4 (right)
Helium plume (VR-density)

Examples of Various Supported Topologies

Hex8

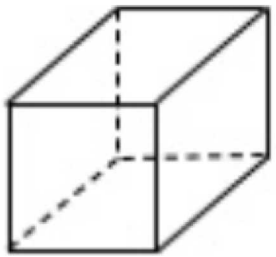

Tet4

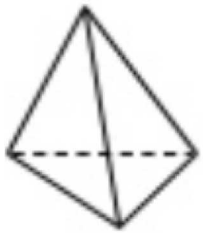

Pyramid5

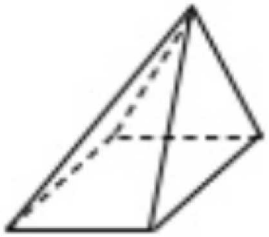

Wedge6

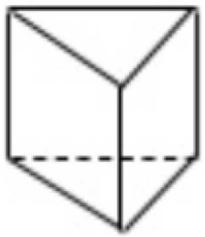

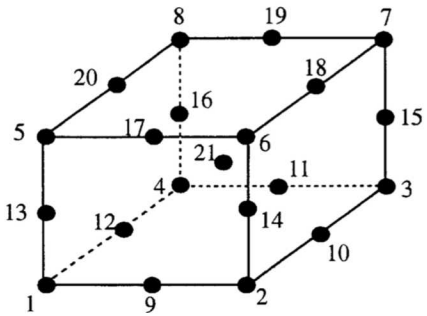

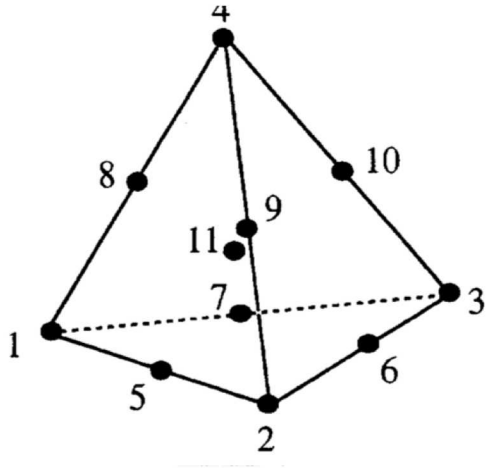

Higher-order promoted elements (Hex27, Tet10)

What About Numerical Quality?

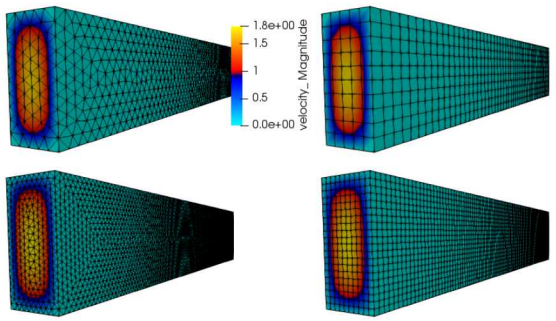

Domino et al., *Comp. & Fluids*, 2019 1x2x10 Findings:

- All topos (Hex8, Hex27, Tet4, Wedge6, Pyramid5) provide design-order accuracy
- Hex8 and Wedge6 provide the same accuracy
- Tet4 results in ~3.5x higher error and matches pyramids
- Higher-order (P=2) notes ~an order of magnitude lower error for the first mesh refinement level (promoted Hex8 R0 mesh)
- Tet4/Pyramid5 O(5)x slower than Hex8/Wedge6 to meet the same accuracy (resource limited model)
- NEW: Tet10 R0 comparable with Hex8 R1

Mesh	R0 Node/Elem	R1 Node/Elem	R2 Node/Elem
Hex8	3,366/2,500	23,331/20,000	173,061/160,000
Hex27	23,331/2,500	173,061/20,000	1,331,721/160,000
Tet4	4,782/23,051	34,418/184,408	260,459/1,475,264
Pyramid5	5,866/15,000	43,331/120,000	333,061/960,000
Wedge6	3,672/5,510	264,99/45,760	197,862/367,240

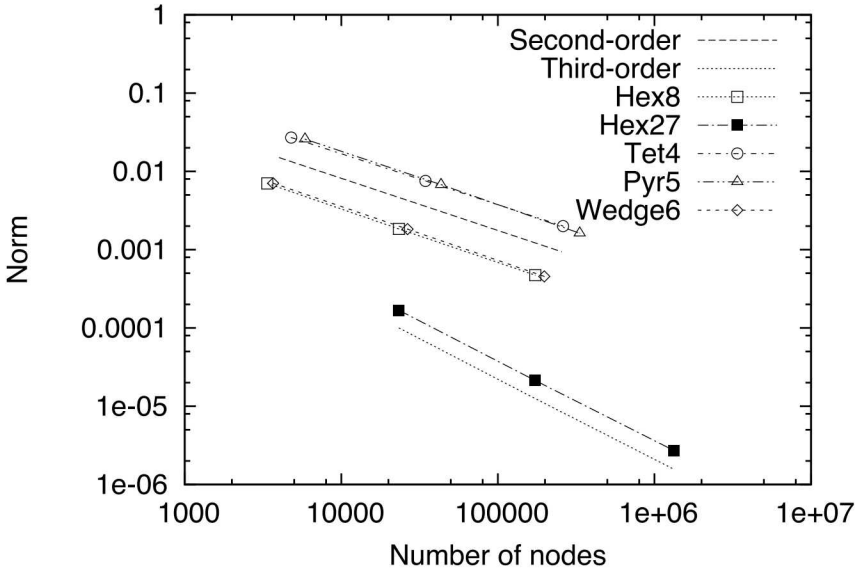

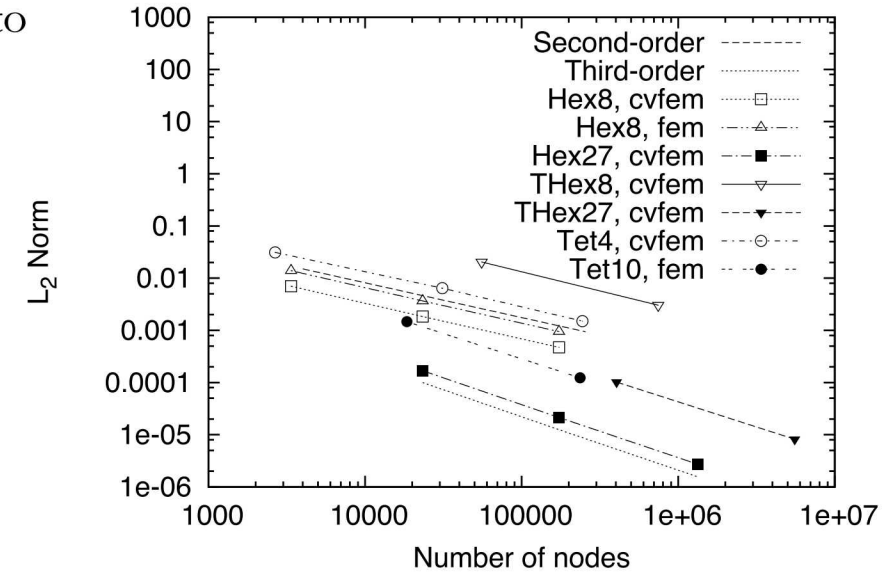

Taylor-Green Vortex (Re 1600)

- Well studied problem that is part of the following numerical benchmark:
  - "C3.5 DNS of the T/G Vortex at Re = 1600"
- QoI: turbulent kinetic energy vs time and dissipation rate vs time
- First phase: small viscous effects, small-scale structures are laminar and organized [easy]
- Second phase: viscous (diffusion) dominates, structures are distorted [harder]
- Break-up phase: flow is dissipating fully [easy]

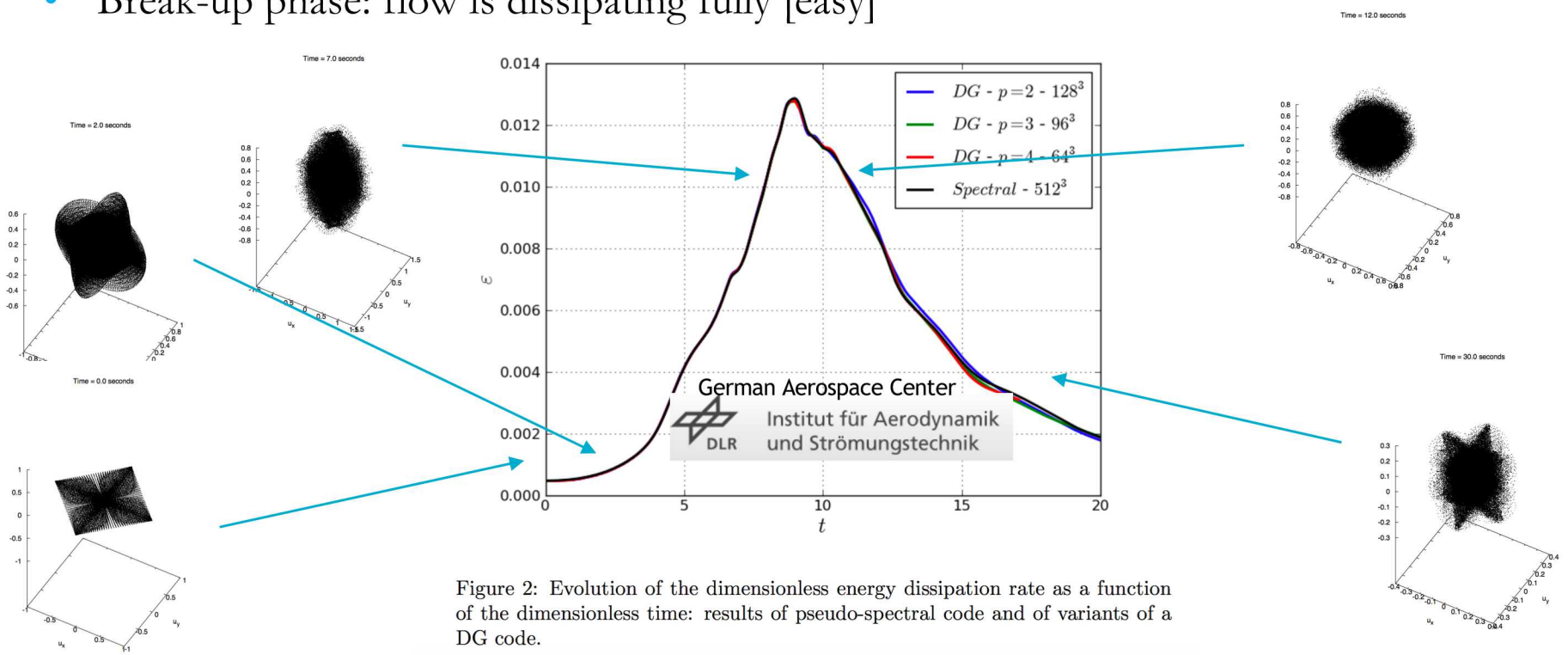

Figure 2: Evolution of the dimensionless energy dissipation rate as a function of the dimensionless time: results of pseudo-spectral code and of variants of a DG code.

Taylor-Green Vortex (Re 1600)

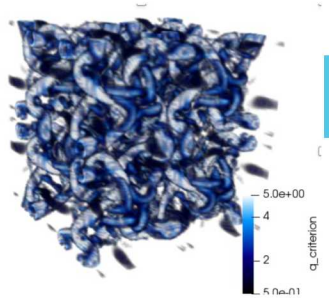

- Visual Comparison

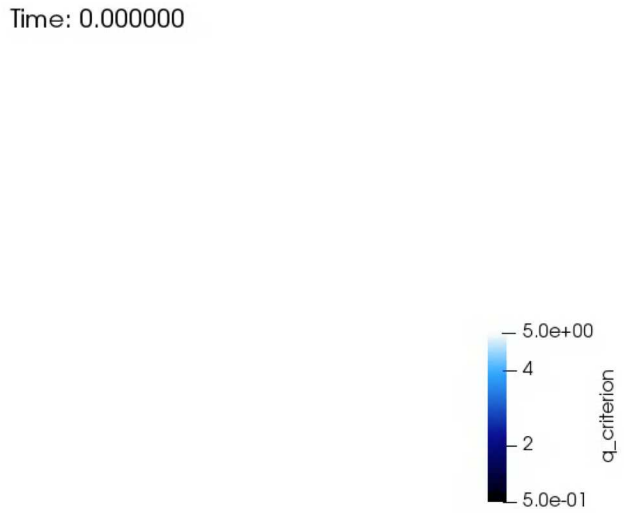

Hex64

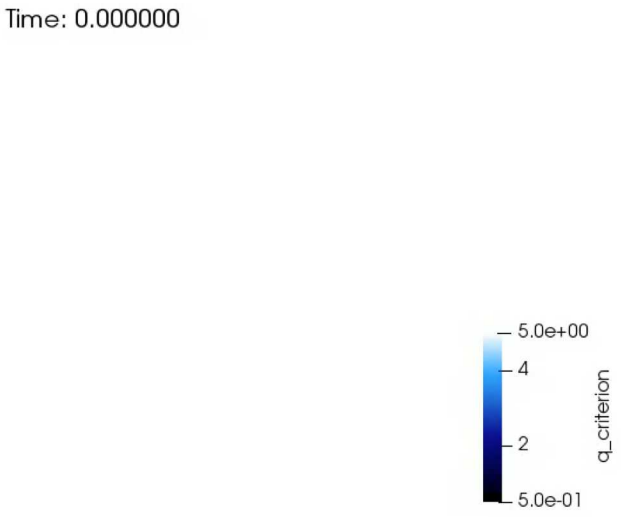

Hex8

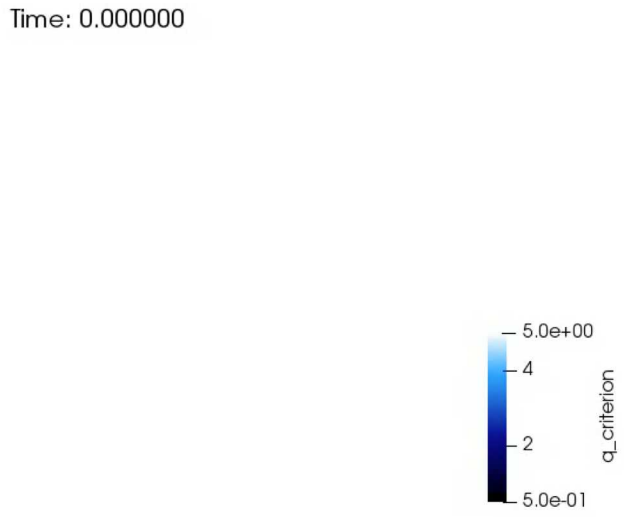

Tet4

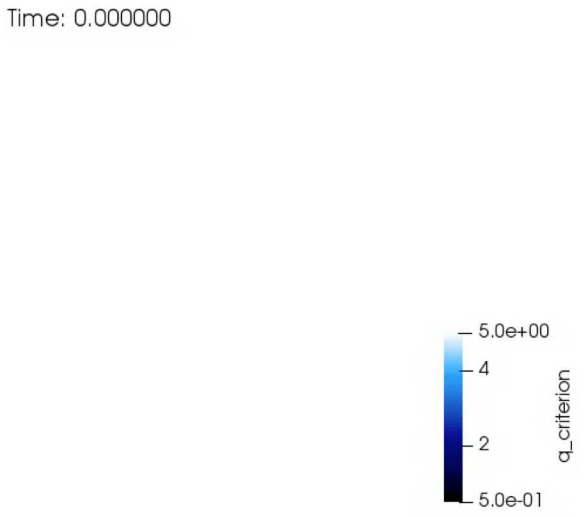

Wedge6

Taylor-Green Vortex (Re 1600) - Results

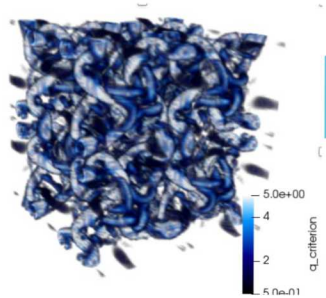

- All topos converge to baseline DNS
- Pyramid5/Wedge6 (at R1) looks very good
- Cost vs Accuracy: P=2 wins

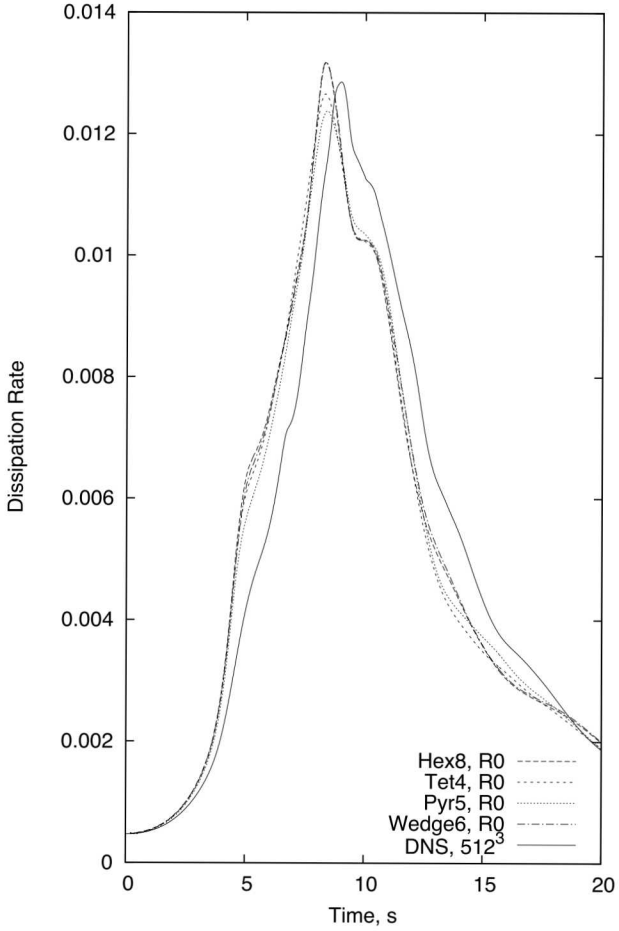

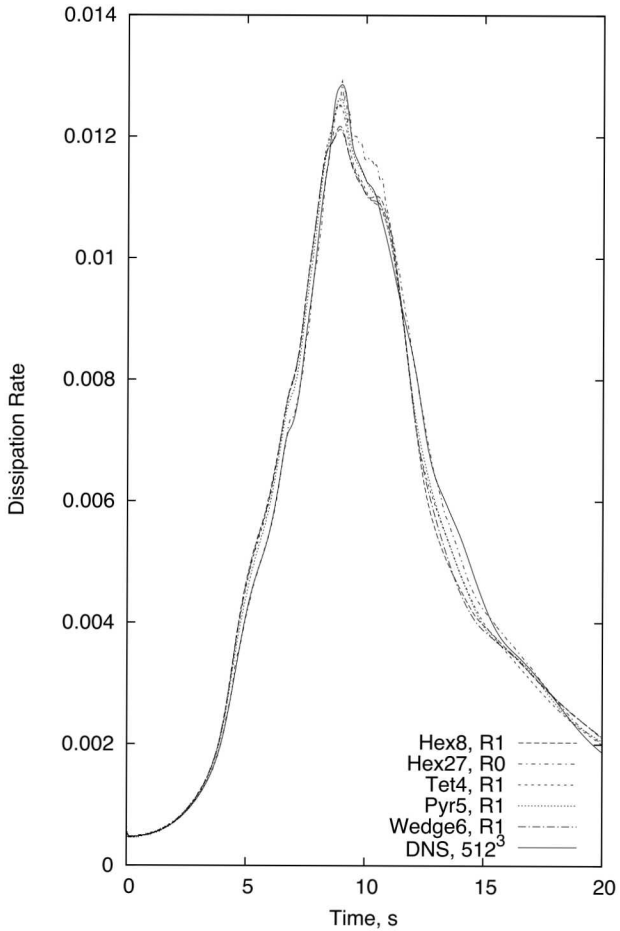

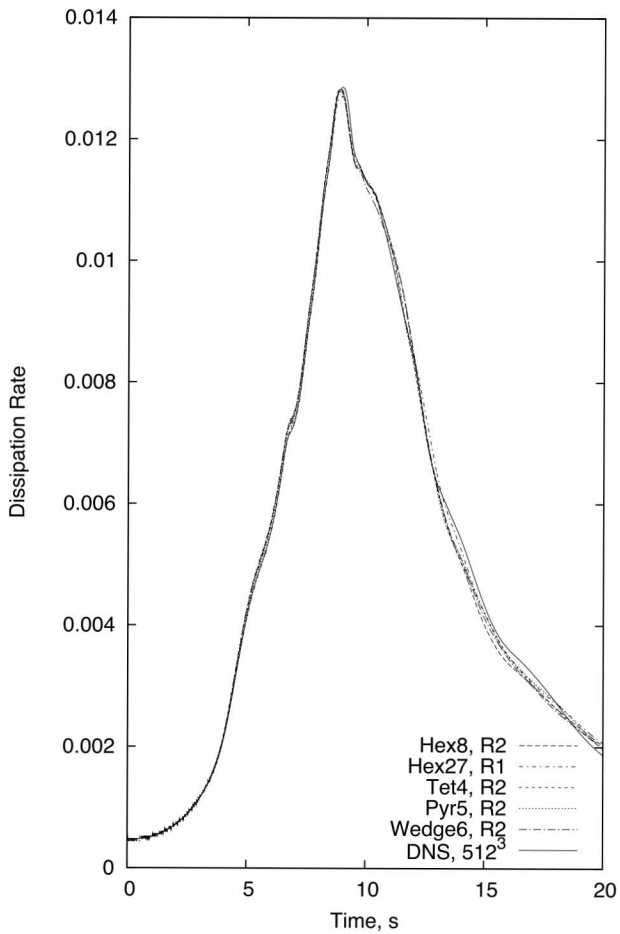

Plain Channel Flow (Re^{τ} 180)

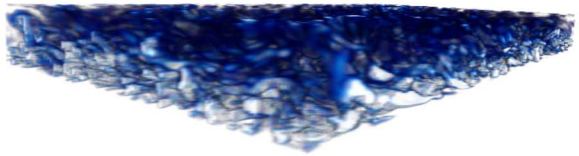

- Hybrid mesh study based on Ham and Iaccarino, *CTR Annual Brief*, 2006, found that simulations were extremely sensitive to mesh topology
  - Non-symmetric time mean flow found for cell-centered; better for the CTR node-centered formulation
- Native CVFEM and EBVC are both symmetric in mean quantities

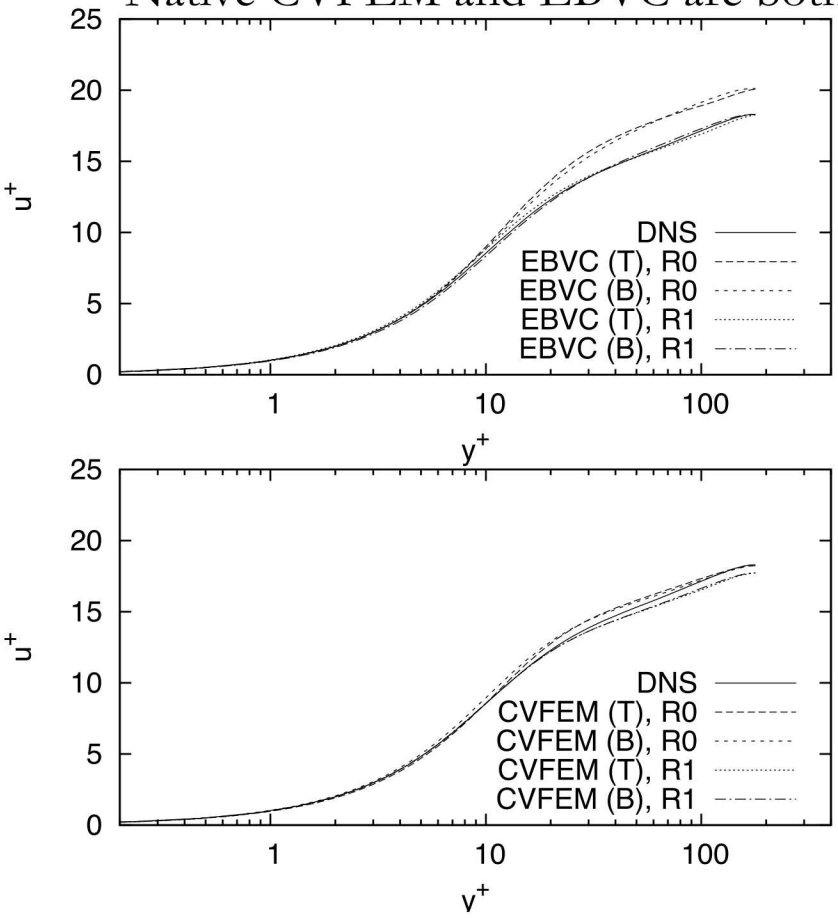

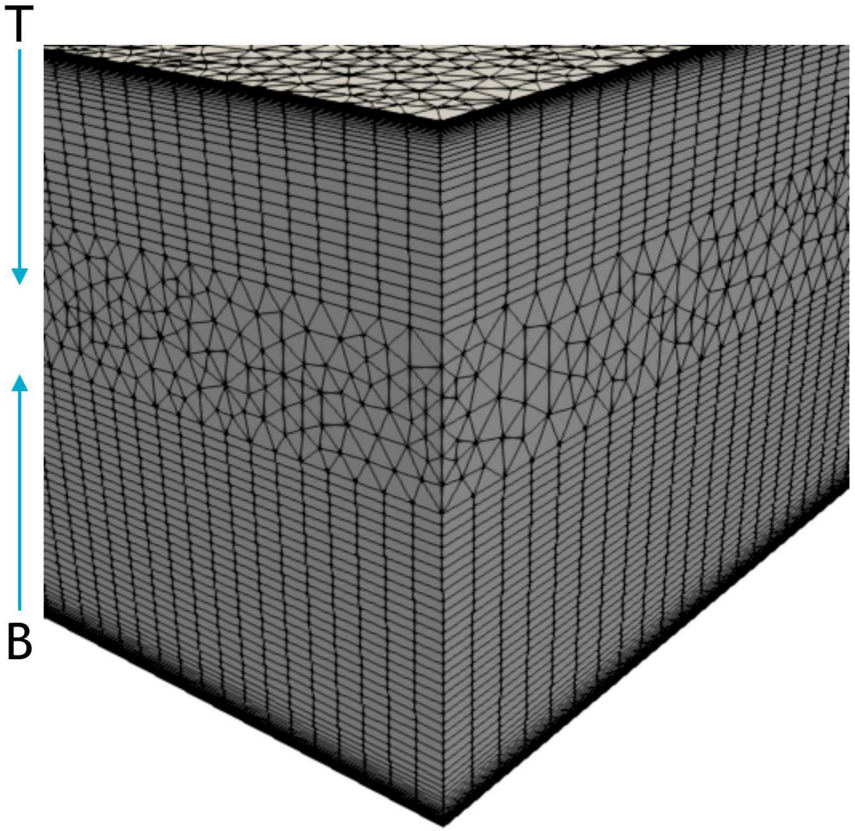

Flow Past Heated Water Channel

- WRLES Ksgs model demonstrates decent mesh convergence (Domino et al. *Comp. & Fluids*, 2019)
- low- and high-order results very similar
- Tet4 simulations are also predicting the flow well at a reduced time.
- Tet10 (not showcased in the paper) is also very promising

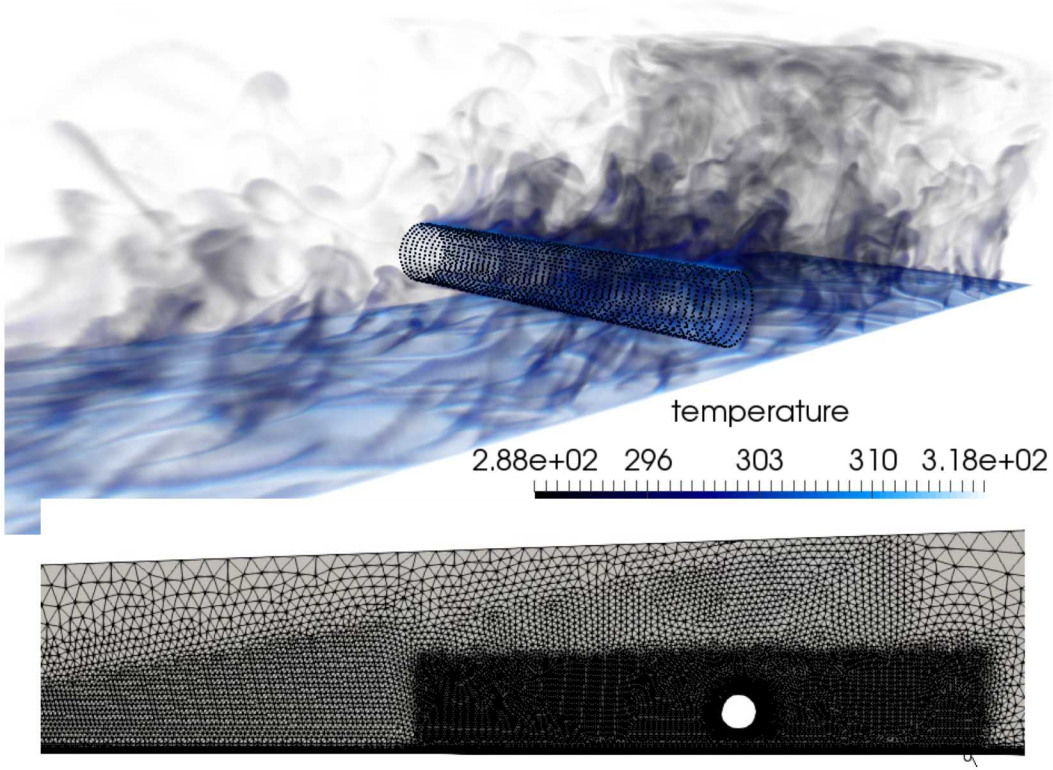

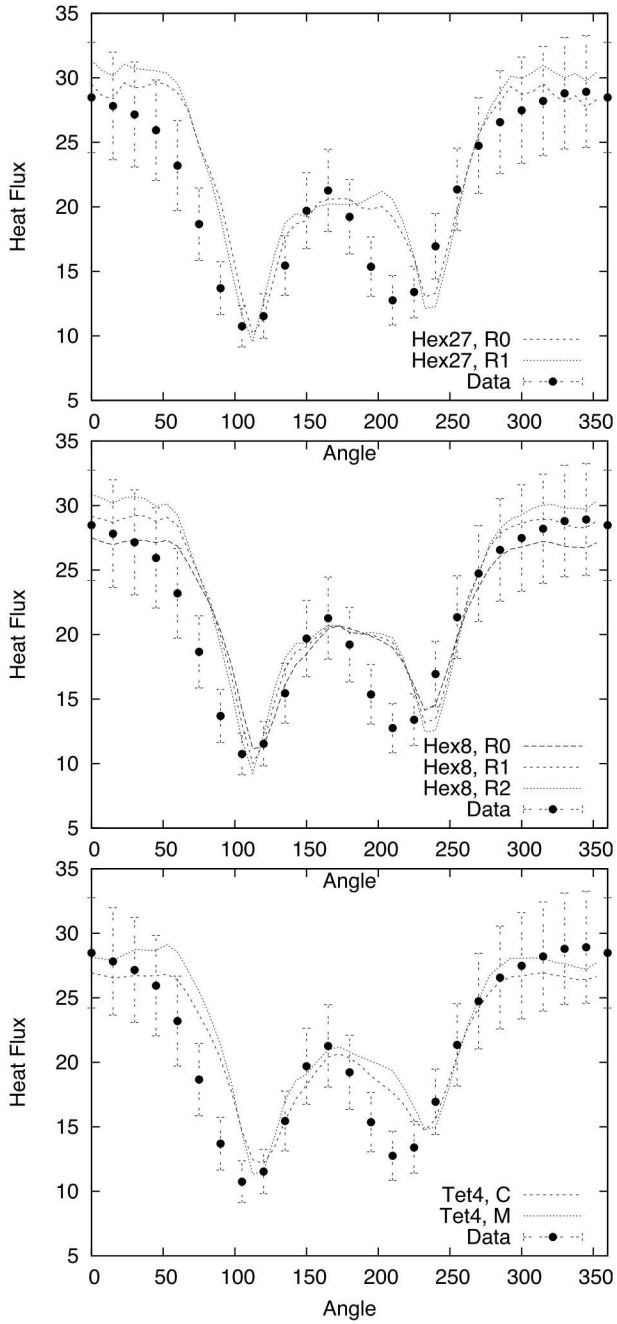

Complex Non-Conformal and Meshing Drivers

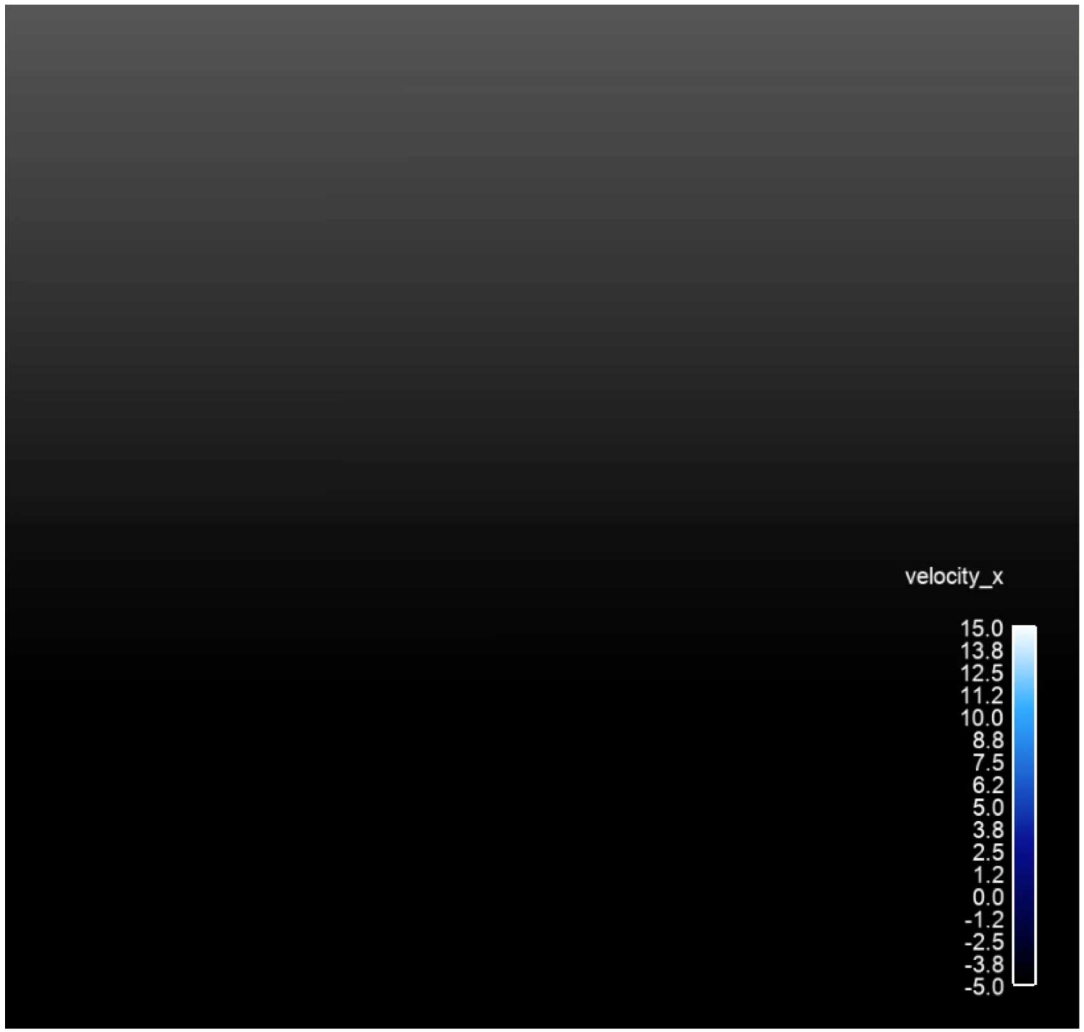

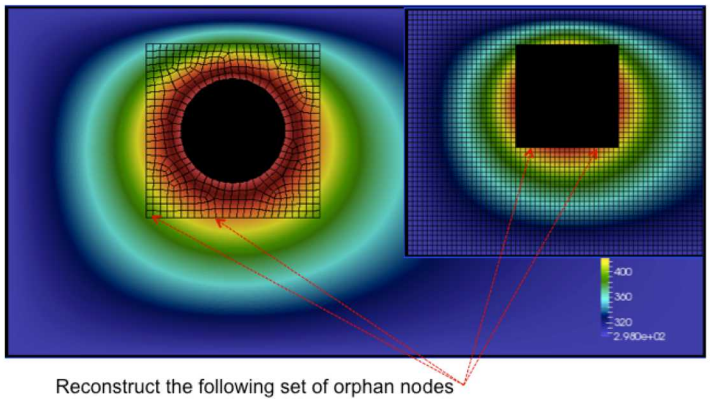

Reconstruct the following set of orphan nodes

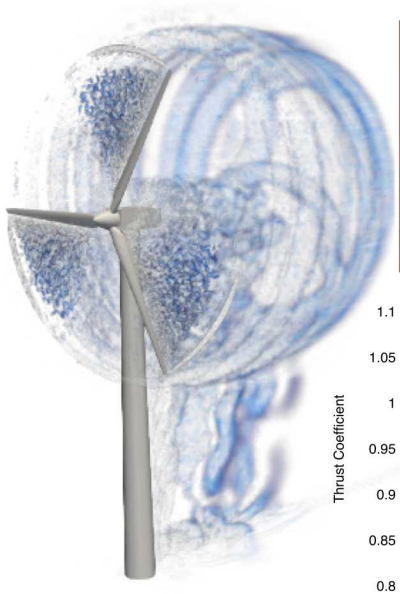

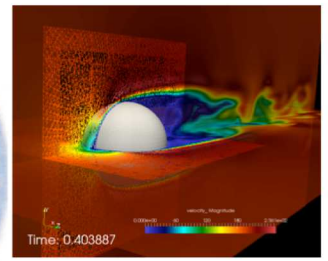

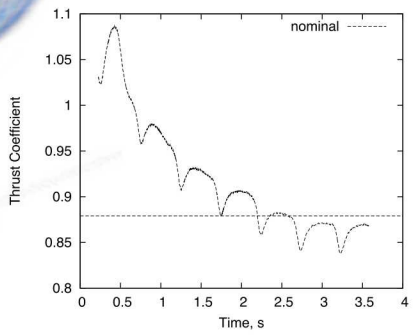

Wind energy applications drive overset and sliding mesh (Vestas V27 225 kW wind turbine simulation), see https://ExaWind.org

Design-order Mesh Constructs for Non-Conformal Interfaces

- Non-conformal and overset methods provides ease of meshing and, when required, mesh motion
- Design-order hybrid DG/CVFEM established, see: Domino, *JCP*, 2018

$$\int_{\Omega_A} w^A \left(\frac{\partial \rho Z}{\partial t} - S_i\right) d\Omega - \int_{\Omega_A} \frac{\partial w^A}{\partial x_j} q_j d\Omega + \int_{\Gamma \setminus \Gamma_{AB}} w^A q_j n_j d\Gamma + \int_{\Gamma_{AB}} w^A \hat{Q}_n(A,B) d\Gamma + \int_{\Gamma_{AB}} \frac{\partial w^A}{\partial x_j} n_j \lambda^{IP} (Z^A - Z^B) d\Gamma, \quad (2.8)$$

and

$$\int_{\Omega_B} w^B \left(\frac{\partial \rho Z}{\partial t} - S_i\right) d\Omega - \int_{\Omega_B} \frac{\partial w^B}{\partial x_j} q_j d\Omega + \int_{\Gamma \setminus \Gamma_{AB}} w^B q_j n_j d\Gamma + \int_{\Gamma_{AB}} w^B \hat{Q}_n(B,A) d\Gamma + \int_{\Gamma_{AB}} \frac{\partial w^B}{\partial x_j} n_j \lambda^{IP} \left(Z^B - Z^A\right)\right) d\Gamma. \quad (2.9)$$

The numerical fluxes, $\hat{Q}_n(\alpha,\beta)$, are

$$\hat{Q}_n(\alpha,\beta) = \frac{1}{2}\left[(q_j^\alpha n_j^\alpha - q_j^\beta n_j^\beta) + \lambda(Z^\alpha - Z^\beta)\right]. \quad (2.10)$$

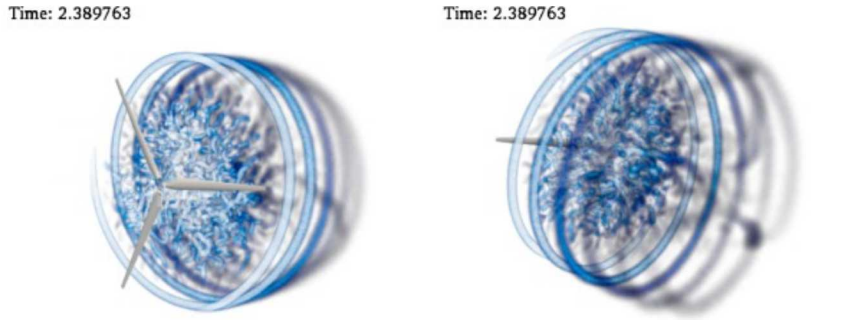

(a) Windward view of the volume rendered Q-criterion.

(b) Leeward view of the volume rendered Q-criterion.

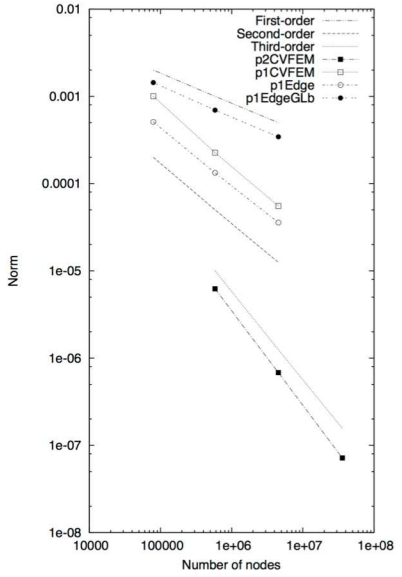

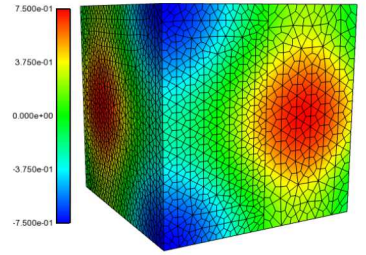

Non-conformal MMS

Scientific Research Platform to Evaluate Higher-Order Methods on Next Generation Platforms

- As the cost of parallel assembly increases, should we strive to perform more local work? Higher-order achieves this design-point (at the cost of a larger memory footprint)
- multi-core KNL-based speed-ups for Kokkos-based kernels (port/perf) demonstrates $P2^{tk} \sim< P1^{tk}$

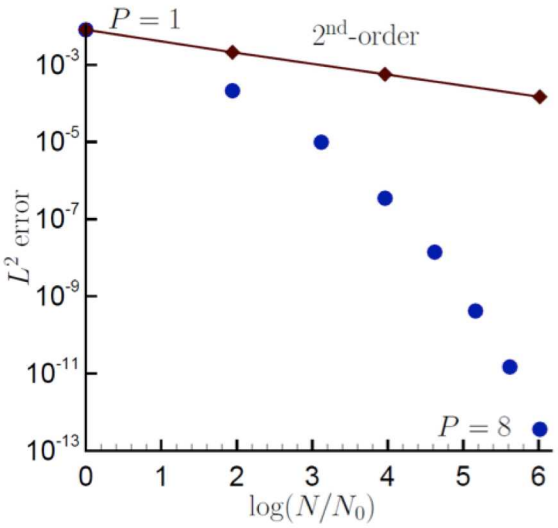

Spectral convergence

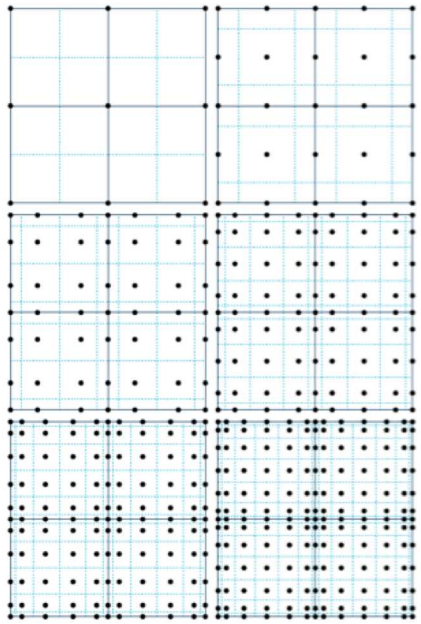

Dual-volume
for promoted quad4

Helium plume comparing
P=1 and P=4

Research Thrust:
Foundational advances for Non-isothermal Impinging Jets

- Systems within the Abnormal Thermal Environment experience pressurization due to internal thermal decomposition of common materials
- At critical component pressures, venting of hot combustible gas occurs either by system design or structural failure
- Venting events are characterized by an impinging turbulent non-isothermal jet blowdown
- Direct Numerical Simulation (DNS) effort is being used to understand low-Mach non-isothermal jet impingement (hot jet, cool surface) heat transfer
- Simulations are being run up to 15 billion mesh nodes on up to 384,000 processors (6000 KNL nodes at 64 MPI-rand/node)
- This DNS is also supporting Machine-learning objectives for, e.g., ML-based wall-modeled LES, and deep neural network authentication methods development

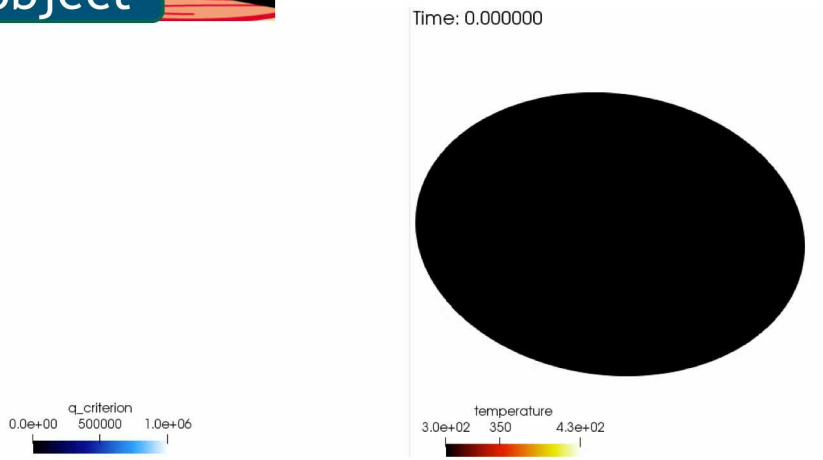

Un-confined impinging jet

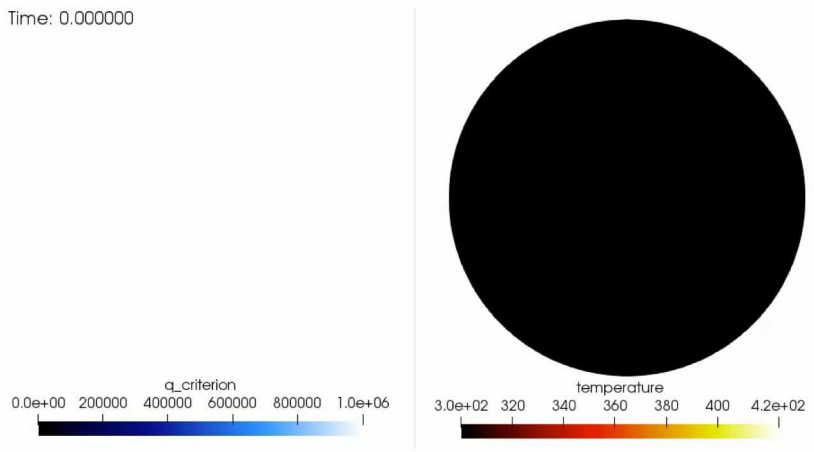

Confined impinging jet

Confined Impinging Jet Challenges

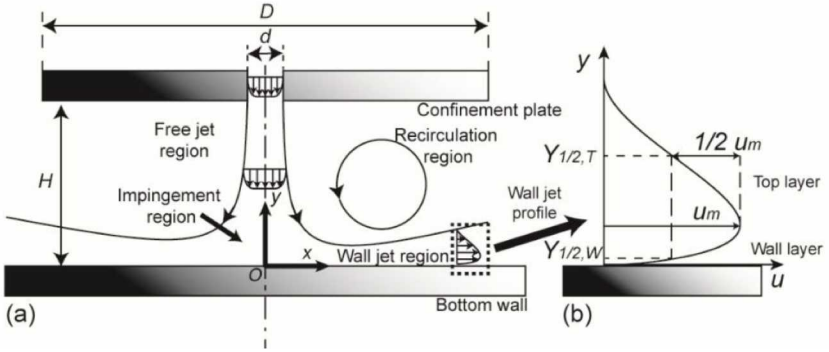

Guo, *Ph.D. Dissertation*, 2013

- Triple-layer structure comprised of:
  - Free-jet region
  - Impinging/stagnation region
  - Wall jet with boundary layer transition and large scale recirculation
- Recirculation region can drastically affect the heat-flux radial profile at the impingement plate
- Flow includes localized high-strain, high-curvature regions, with near-stagnation point negative turbulent production of kinetic energy breaks RANS and LES

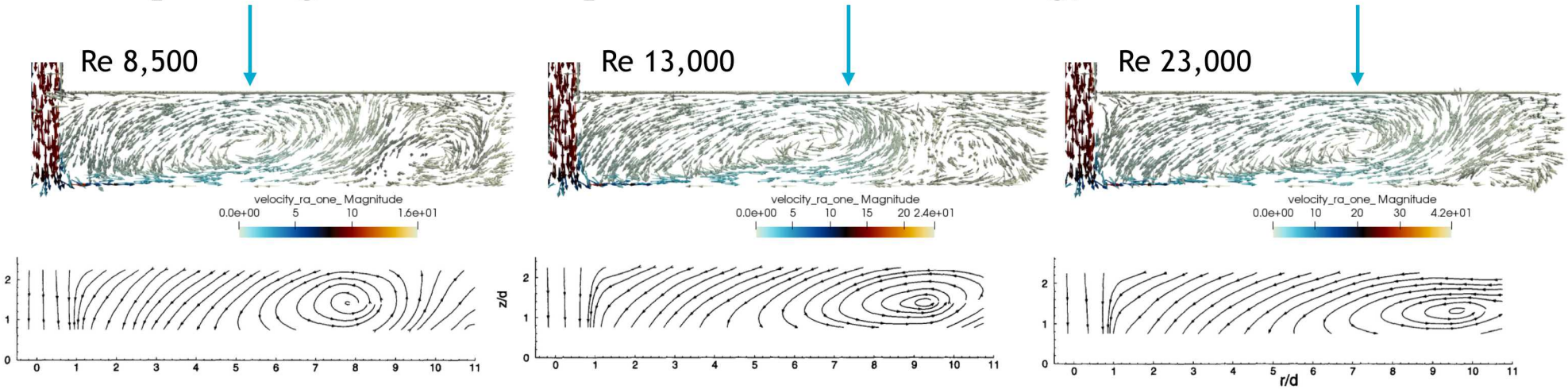

(top) current WALE-WMLES study (Domino, 2020)
(bottom) Fitzgerald and Garimella, *Int. J. Heat Mass Transfer*, 1998

Re ~10,000 DNS Impinging Jet Simulation Study

Volume-rendered Q-criterion and barycentric map

- Four inlet jet temperatures (25C, 100C, 300C, and 600C)
  - Gap height / jet dimeter; H/D = 3
  - Jet radius / domain diameter; R/D = 15
  - Near-wall pipe and impingement plate resolution, 10^{-5} m
  - Bulk region near Kolmogorov length scale ~0.01 mm
  - Base mesh ~1.8 billion Hex8 elements
  - Refined mesh in P ~ 15 billion nodes, Hex27 mesh; ~800 gig
- DNS pipe flow precursor ($Re^{\tau} = 505$) provides inflow condition

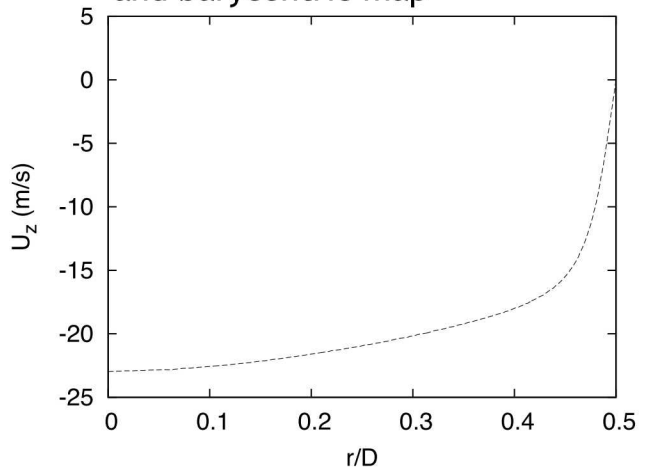

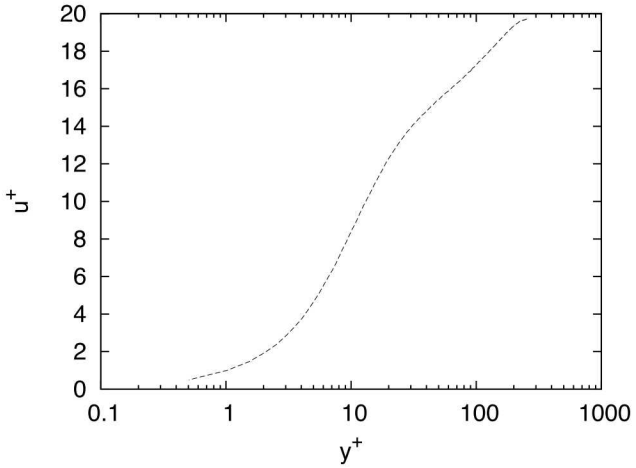

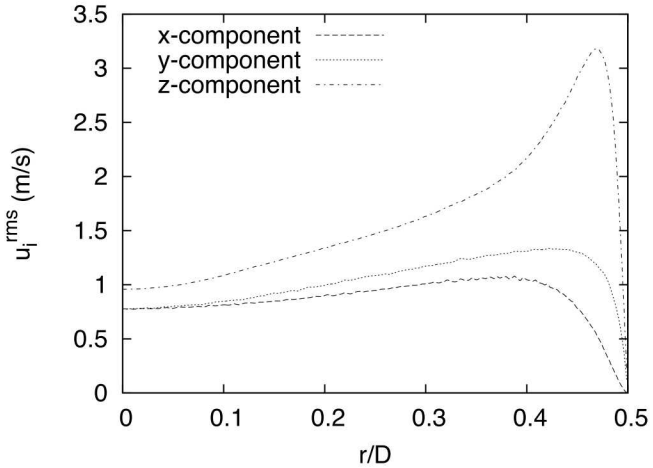

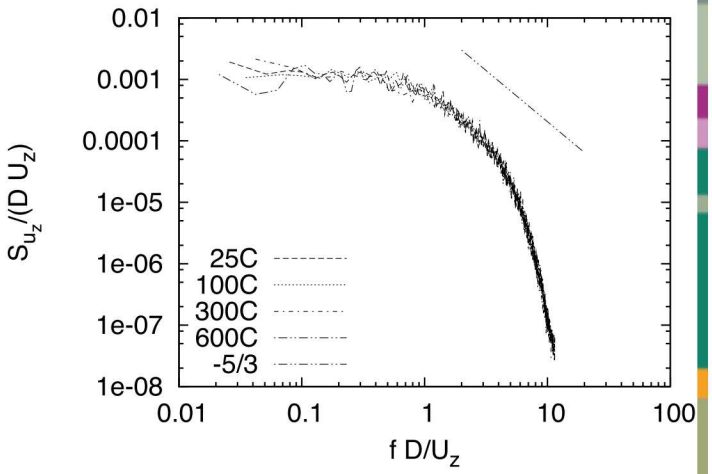

Re ~10,000 DNS Impinging Jet Simulation Study (preliminary)

- 25C and 100C nearly complete (statistics)

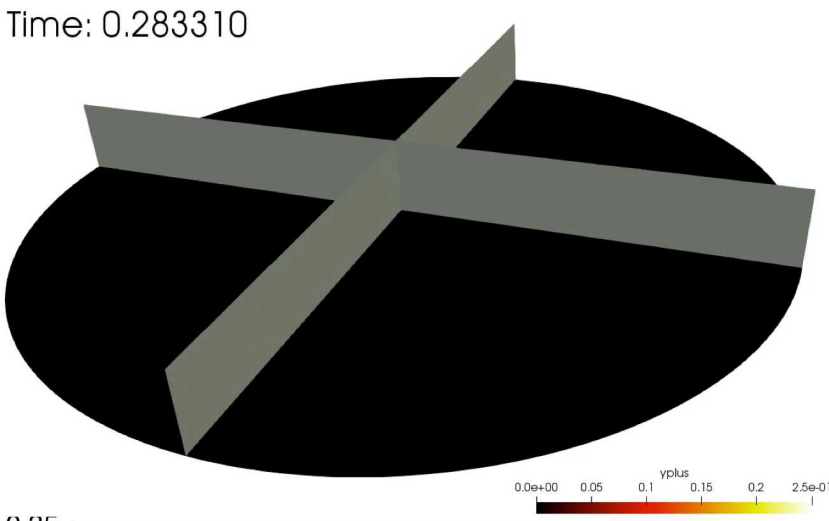

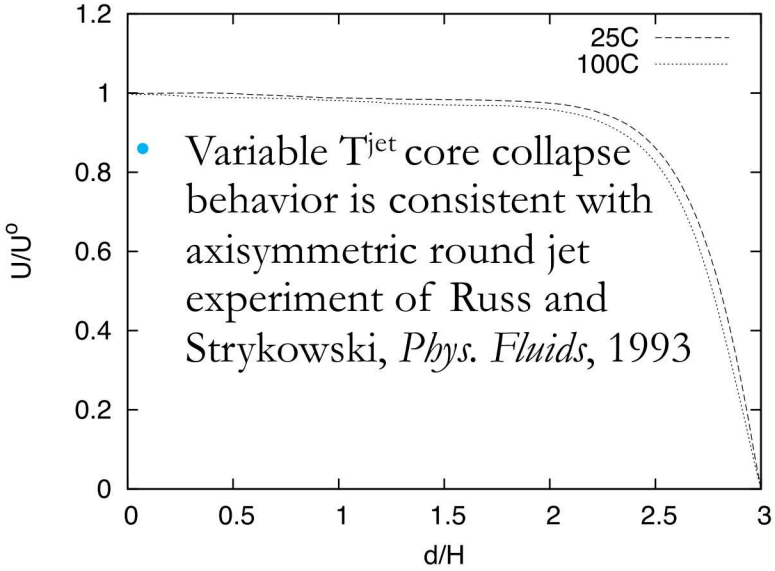

- Variable T^{jet} core collapse behavior is consistent with axisymmetric round jet experiment of Russ and Strykowski, *Phys. Fluids*, 1993

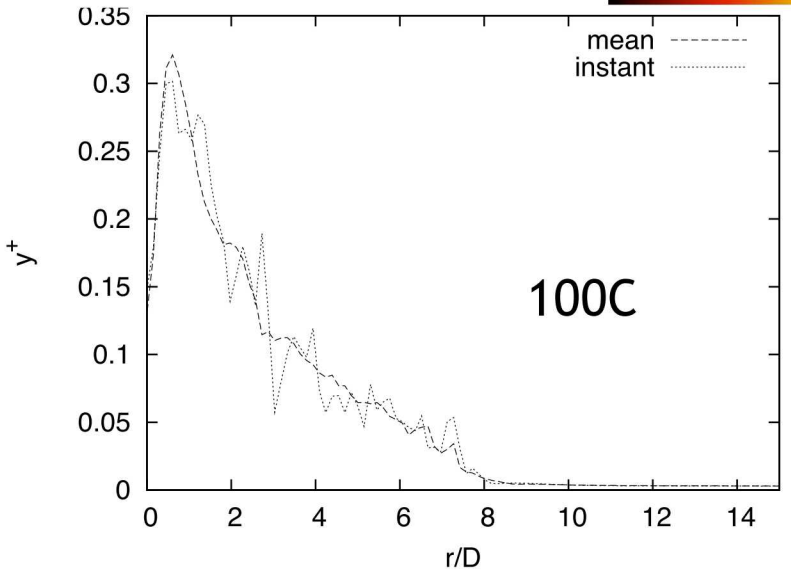

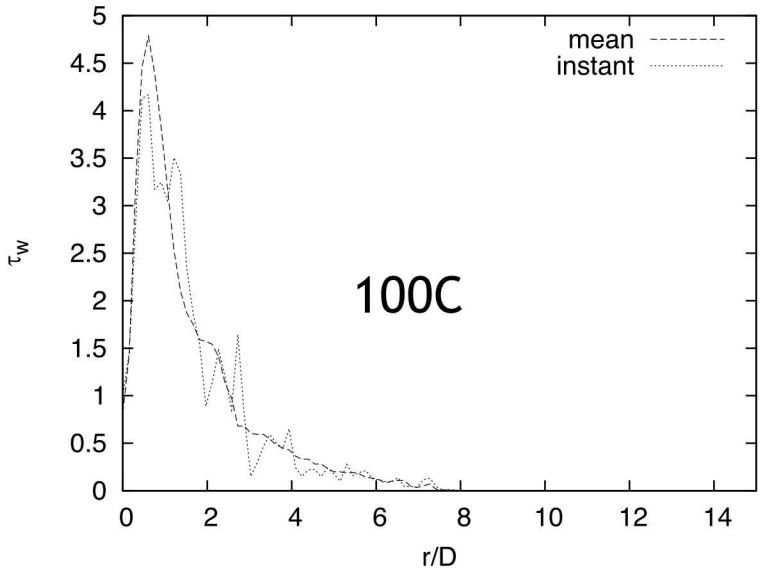

Research Thrust: Impinging Jet Fluid Mechanics in the Presence of Clutter

- Real systems include clutter and jet impingement obstructions that can drastically affect the flow pattern
- Complex geometries require generalized unstructured or high-order tetrahedral capability
- Tet-based WMLES approach shown below with entrance pipe region
  - Expected proposal for joint experimental and numerical design project

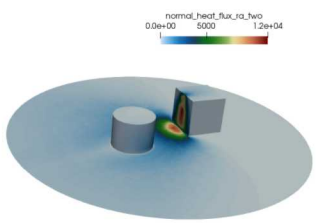

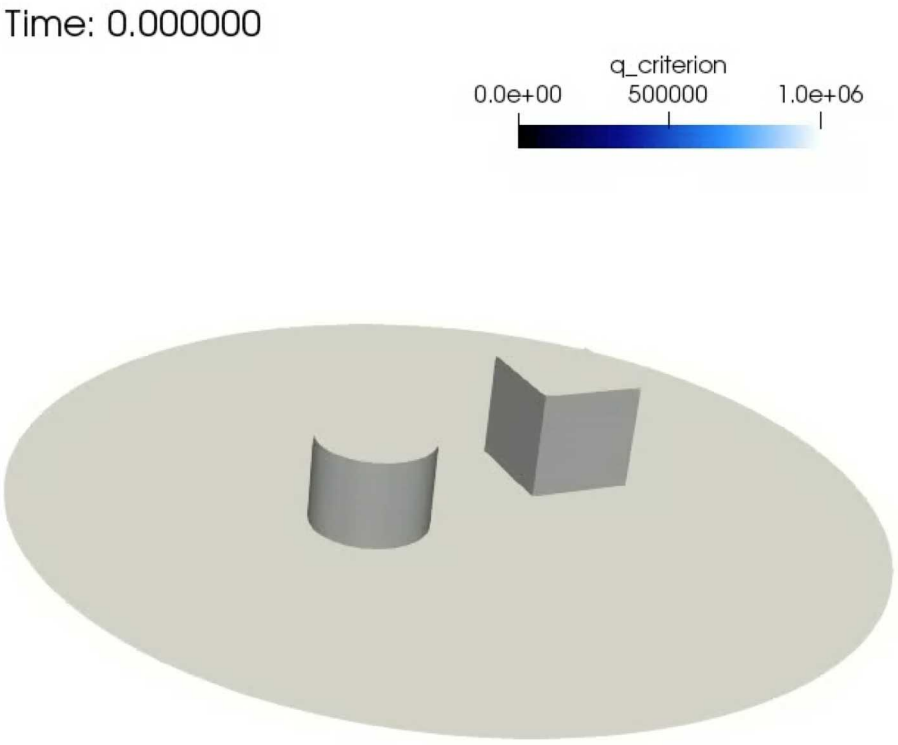

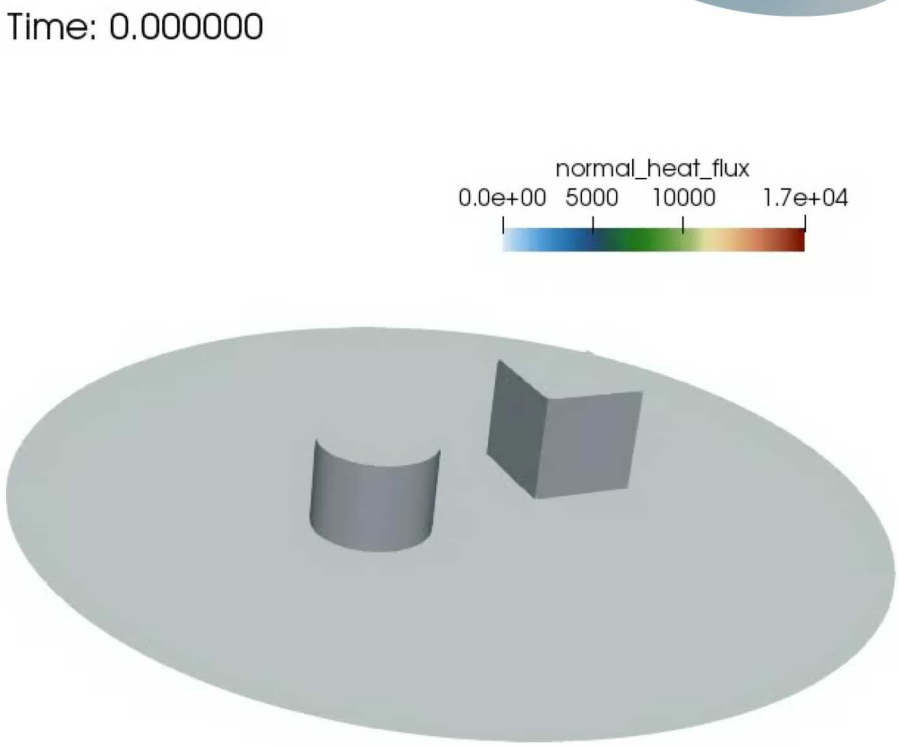

Research Thrust: Partnership with Dr. Matthew Barone, 1515 Near-wall Turbulence Modeling in Large Eddy Simulation

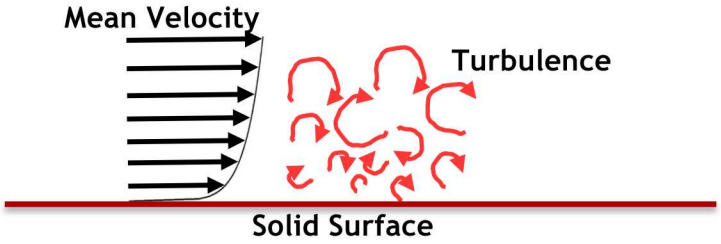

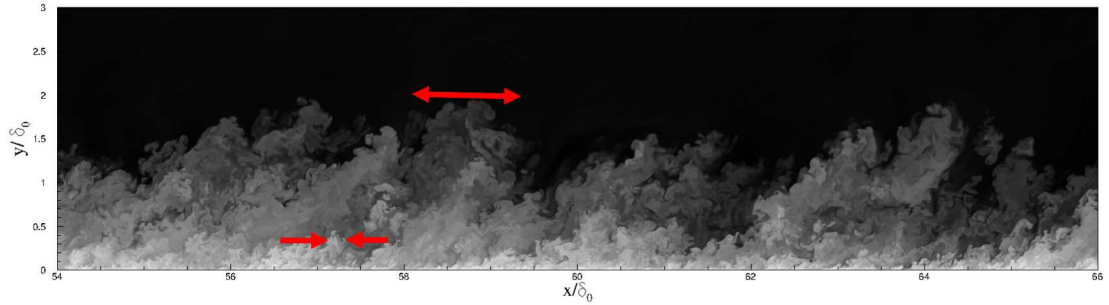

Notional Direct Numerical Simulation (DNS) mesh

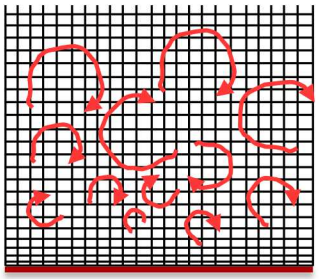

Notional LES mesh

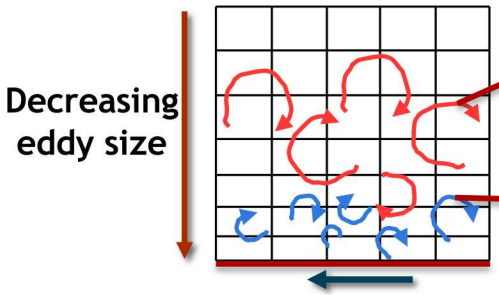

$$\tau(\boldsymbol{x}, t) = F(\boldsymbol{U}, d, ?, ?, \ldots)$$

Wall-modeled LES offers computational savings decrease of *at least* several orders of magnitude over DNS for engineering systems of interest.

$DNS \sim Re^{3}$ $LES^{outer} \sim Re^{0.4}$ $WRLES \sim Re^{1.8}$ Chapman, *AIAA J.*, 1979

The Research Question

Key Premise

New near-wall turbulence models based on traditional approaches - theory, phenomenology, and limited calibration to data - will not result in significant improvements in predictive accuracy for surface loading simulations.

Research Question

Can ***data-driven models***, constructed using ***machine learning techniques***, provide a novel path forward for near-wall turbulence models with improved accuracy for surface loading predictions?

Decision Tree/Random Forest

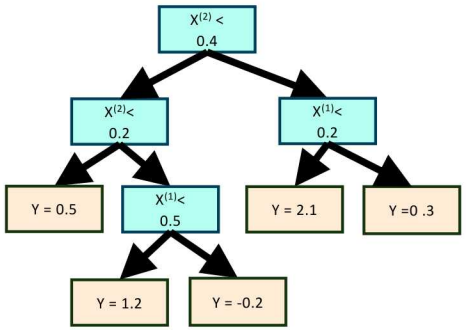

Neural Network, or Multi-Layer Perceptron (MLP)

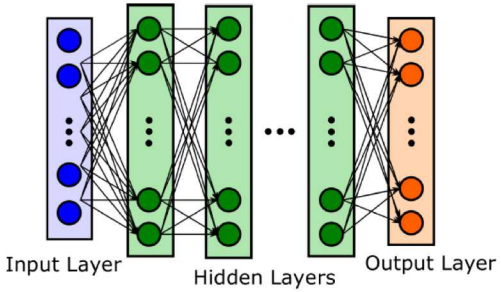

Constructing a Coordinate-Frame Invariant Near-Wall Turbulence Model [1]

- The wall shear stress model must be applicable for:
  - Arbitrary Cartesian coordinate system
  - Arbitrary orientation of the wall

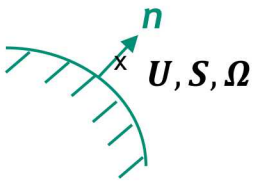

- This fundamental property is ensured by using tensor invariant theory to identify:
  - The appropriate invariant features (inputs) to the model
  - A representation of the wall shear stress vector invariant to rotations about the wall-normal vector

Scalar invariant inputs

$$\lambda_1 = \{\overline{\mathbf{S}}\}, \qquad \lambda_2 = \{\overline{\mathbf{S}}^2\},$$
$$\lambda_3 = \{\overline{\mathbf{\Omega}}^2\}, \qquad \lambda_4 = \{\overline{\mathbf{S}}^3\},$$
$$\lambda_5 = \{\overline{\mathbf{S}}\,\overline{\mathbf{\Omega}}^2\}, \qquad \lambda_6 = \overline{\mathbf{U}} \cdot \overline{\mathbf{U}},$$
$$\lambda_7 = \overline{\mathbf{U}} \cdot \overline{\mathbf{S}}\,\overline{\mathbf{U}}, \qquad \lambda_8 = \overline{\mathbf{U}} \cdot \epsilon\overline{\mathbf{\Omega}},$$
$$\lambda_9 = \mathbf{n} \cdot \overline{\mathbf{S}}\mathbf{n}, \qquad \lambda_{10} = \mathbf{n} \cdot \overline{\mathbf{U}},$$
$$\lambda_{11} = \mathbf{n} \cdot \epsilon\overline{\mathbf{\Omega}}, \qquad \lambda_{12} = \mathbf{n} \cdot \overline{\mathbf{S}}^2\mathbf{n},$$
$$\lambda_{13} = \mathbf{n} \cdot \epsilon\overline{\mathbf{S}}\,\overline{\mathbf{\Omega}}, \qquad \lambda_{14} = \mathbf{n} \cdot (\overline{\mathbf{S}}\mathbf{n} \times \overline{\mathbf{S}}^2\mathbf{n}),$$
$$\lambda_{15} = \mathbf{n} \cdot \epsilon\overline{\mathbf{S}}\,\overline{\mathbf{\Omega}}^2, \qquad \lambda_{16} = \mathbf{n} \cdot \overline{\mathbf{S}}\,\overline{\mathbf{\Omega}}\mathbf{n},$$
$$\lambda_{17} = \mathbf{n} \cdot \overline{\mathbf{S}}\,\overline{\mathbf{U}}, \qquad \lambda_{18} = \mathbf{n} \cdot (\overline{\mathbf{U}} \times \overline{\mathbf{S}}\,\overline{\mathbf{U}}),$$
$$\lambda_{19} = \mathbf{n} \cdot (\overline{\mathbf{U}} \times \overline{\mathbf{S}}\mathbf{n}), \qquad \lambda_{20} = \mathbf{n} \cdot \overline{\mathbf{\Omega}}\,\overline{\mathbf{U}},$$

Form invariant inputs (vectors)

$$\Pi^{(1)} = \overline{\mathbf{U}}, \qquad \Pi^{(2)} = \epsilon\overline{\mathbf{\Omega}},$$
$$\Pi^{(3)} = \mathbf{n}, \qquad \Pi^{(4)} = \overline{\mathbf{S}}\mathbf{n},$$
$$\Pi^{(5)} = \mathbf{n} \times \overline{\mathbf{S}}\mathbf{n}, \qquad \Pi^{(6)} = \overline{\mathbf{\Omega}}\mathbf{n},$$
$$\Pi^{(7)} = \mathbf{n} \times \overline{\mathbf{U}}, \qquad \Pi^{(8)} = \mathbf{n} \times \overline{\mathbf{\Omega}}\mathbf{n}.$$

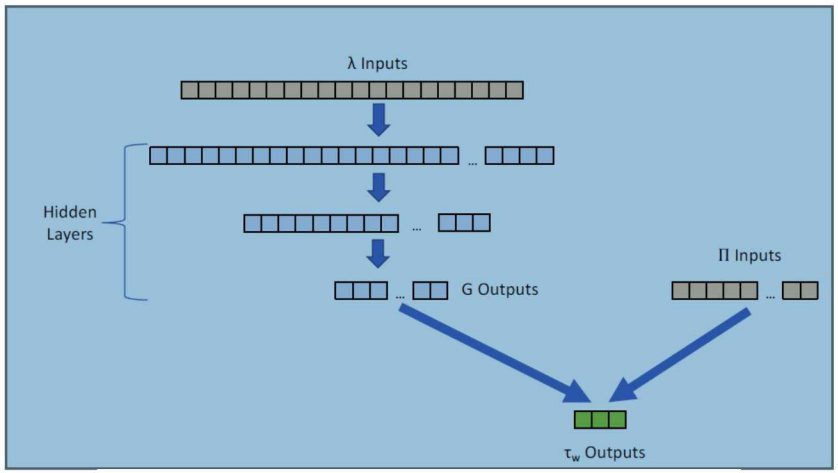

$$\begin{bmatrix} \tau_{w,1} \\ \tau_{w,2} \\ \tau_{w,3} \end{bmatrix} = \begin{bmatrix} \Pi_1^{(1)} & \Pi_1^{(2)} & \Pi_1^{(3)} & \cdots & \Pi_1^{(8)} \\ \Pi_2^{(1)} & \Pi_2^{(2)} & \Pi_2^{(3)} & \cdots & \Pi_2^{(8)} \\ \Pi_3^{(1)} & \Pi_3^{(2)} & \Pi_3^{(3)} & \cdots & \Pi_3^{(8)} \end{bmatrix} \begin{bmatrix} G^{(1)} \\ G^{(2)} \\ G^{(3)} \\ \vdots \\ G^{(8)} \end{bmatrix}$$

[1] Inspired by Ling, Kurzawski, and Templeton, "Reynolds averaged turbulence modelling using deep neural networks with embedded invariance." *J. Fluid Mech.* 807:155-166, 2016.

A Priori Tests of the ML Wall Shear Stress Model

Training Data

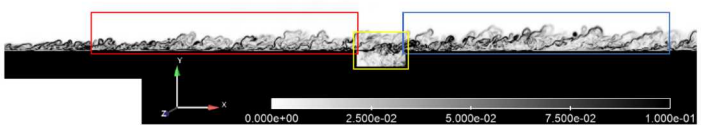

Test Case

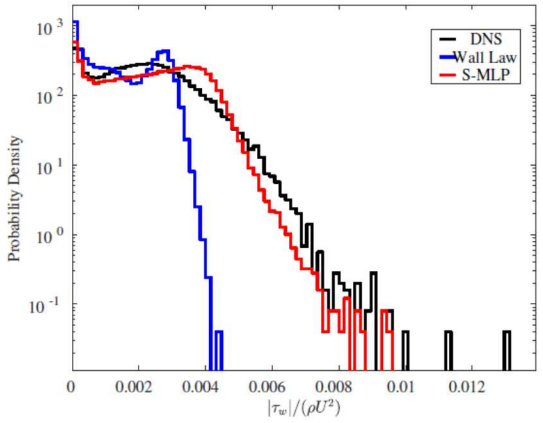

a) $|\tau_w|$

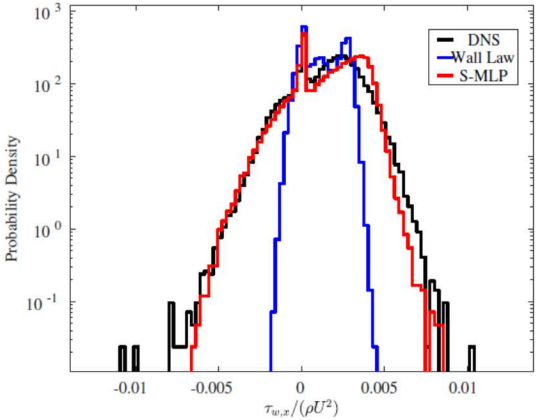

b) $\tau_{w,x}$

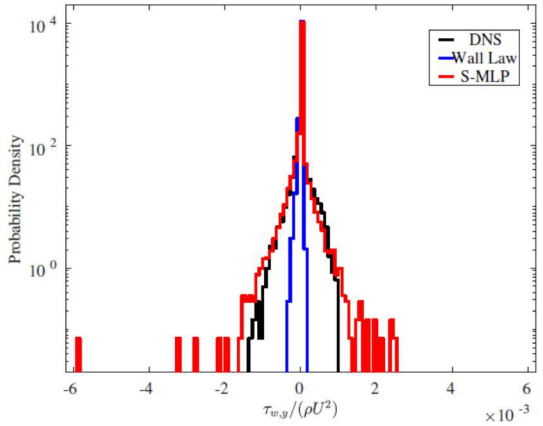

c) $\tau_{w,y}$

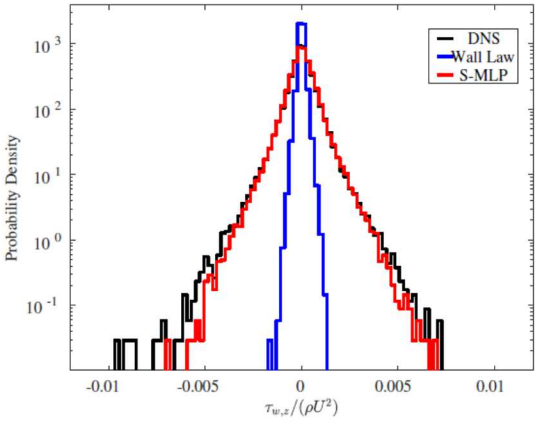

d) $\tau_{w,z}$

Conclusions

- The dynamics of fire is a multi-physics and highly non-linear
- As crossflow increases, the likelihood of whirling fire events increases
- Damaged bodies/clutter (not discussed) also increases mixing and, hence,
- Coupling low-Mach reacting flow with PMR and CHT requires stable and accurate operator split approaches
- Quality numerical methods deployment is required to ensure stable, accurate, and convergent analysis especially when applied to complex geometries
- A quality VVUQ effort includes assessment of numerical accuracy, model-form uncertainties, and evaluation of the assumed physics
- Automatic uncertainty approaches for LES are developing
- DNS can provide valuable insight to complex physics, especially, when capability computing is deployed
- Machine learning approaches are being evaluated and developed for wall-modeled LES

Acknowledgements

Funding:

- ASC Integrated Codes, Physics and Engineering Models, and Verification and Validation portfolios
- Exascale Computing Project (17-SC-20-SC)
- Sandia National Laboratories Staff:
  - Dr. Alex Brown (square quiescent fire simulation)
  - Dr. Sarah Scott (fire in cross flow activities)
  - Dr. Matt Barone (machine-learning research thrust)

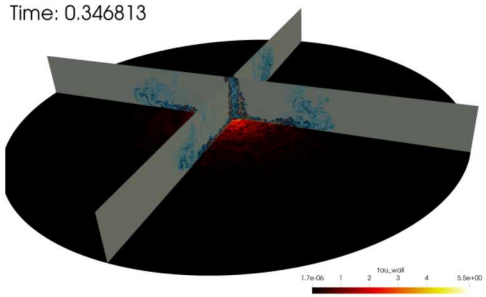

"Indeed, all I can say to you at the end of these lectures (for we must come to an end at one time or other) is to express a wish that you may, in your generation, be fit to compare to a candle; that your may like it, shine as lights to those about you; that, in all your actions, you may justify the beauty of the taper by making your deeds honorable and effectual in the discharge of your duty to your fellow-men."

The Chemical History of a Candle, Michael Faraday (1791-1867)

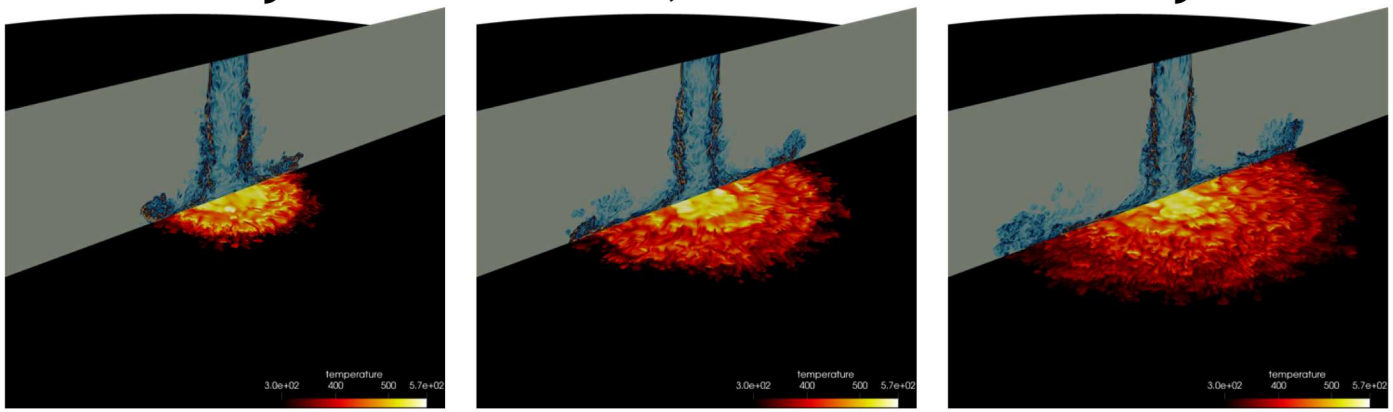

Vertical plane of vorticity shadings with near-wall impingement plane of temperature shadings for the 300C inlet jet temperature. For this jet sequence, six restarts were required (each using the full 24-hour Trinity KNL run time limit).

Seminar Announcement

Title: An Evolution of a Mindset: A Historical Perspective on Sandia National Laboratories Fire Science Philosophy

Abstract:

Sandia National Laboratories continues to develop and deploy a comprehensive experimental, modeling, and simulation program whose goal is to drive foundational advancements in fire physics understanding. The abnormal thermal environment, which is classically characterized as a highly sooting hydrocarbon combustion event, arises during an accident scenario in which a breached liquid inventory reacts. Fully or partly engulfed objects subjected to an abnormal thermal environment are both radiatively and convectively heated. This multi-physics event can be defined as a low-Mach, turbulent reacting flow coupled to soot transport, thermal radiation, and thermal response. Accident use-cases that include propellants or carbon fiber-based materials add Eulerian/point-particle Lagrangian physics and/or heterogenous combustion coupling, respectively. In fact, over the past three decades, representative accident scenarios of interest have changed. For example, early use-cases focused on large-scale hydrocarbon outdoor pool fires (JP-8) in quiescent conditions. Recent experimental and theoretical research efforts have demonstrated that the inclusion of an environmental cross-flow dramatically augments heat loading to objects due to increased fuel/air mixing efficiency that counter-rotating vortex structures provide. In the most extreme case, fire whirls are present. Fire whirling phenomena are characterized by tornadic-like fluid pockets of reacting flow whose formation is dictated by the coupling of buoyant acceleration from the fire in the presence of environmental cross flow.

In this presentation, a history of fire physics understanding at Sandia National Laboratories Engineering Science Center will be provided. This journey will describe an evolution of mindset in fire mechanics understanding whose inception shares lineage with "The Chemical History of a Candle" [1] and extends to complex fire whirling behavior. The link between this evolution of a mindset/understanding and required experimental, modeling, and simulation pathways will be outlined. Fire experimental and simulation findings will be provided, in addition to an overview of fire physics fundamentals. The presentation will also include recent verification and validation research findings and numerical advances that map to a required fluid mechanics paradigm shift: blunt transition from Reynolds- Averaged Navier-Stokes (RANS) approaches to the incorporation of higher-fidelity turbulence simulation constructs such a large-eddy simulation (LES) and direct numerical simulation (DNS). Finally, future research paths will be outlined including accurate, low-dissipation low-Mach methods, VVUQ methods, and machine-learned wall-modeled LES appraoches.

[1] The Chemical History of a Candle, Michael Faraday, Royal Institution "Christmas lectures for young people", 1825.